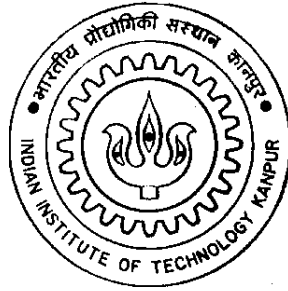


HOMOGENIZATION BASED DAMAGE MODEL
FOR UNIDIRECTIONAL COMPOSITES
WITH
TRANSVERSE MATRIX CRACKS

by

A Y Santosh



DEPARTMENT OF AEROSPACE ENGINEERING
INDIAN INSTITUTE OF TECHNOLOGY KANPUR

June, 2011

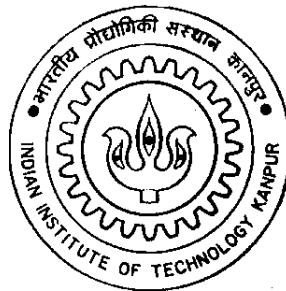
**HOMOGENIZATION BASED DAMAGE MODEL
FOR UNIDIRECTIONAL COMPOSITES
WITH
TRANSVERSE MATRIX CRACKS**

A Thesis Submitted
in Partial Fulfillment of the Requirements
for the Degree of

MASTER OF TECHNOLOGY

by

A Y Santosh



DEPARTMENT OF AEROSPACE ENGINEERING
INDIAN INSTITUTE OF TECHNOLOGY KANPUR

June, 2011

Dedicated to

My Parents, Friends and Professors

whose influences

have made me

the person I am today

ACKNOWLEDGEMENT

I would like to express my sincere gratitude to my thesis advisor Dr. C. S. Upadhyay without his support this experience would have not been possible. I will always be thankful for his understanding nature and the amount of freedom he has provided me along the course of this research. It has been a wonderful learning experience attending his courses and working with him. All the learning from this association will be of great help to me in my future endeavors.

I am extremely thankful to the faculty of the Indian Institute of Technology Kanpur, who have taught me and made my journey from a school student to an engineer a memorable one.

It was a pleasure to be associated with the Structures Lab of the Aerospace Department. A special note of thanks is due to V. Murari for sharing his piece of work for my research, his kind support towards all my problems, technical discussions and the valuable suggestions, without which, this work would lack a lot of quality.

I would like to thank all my friends: Shinu, Arunabha, Navrose, Dharmendra, Harish, Nithesh, Sudipta, Kuldeep, Shyam and Praveen for their kind support. I am greatly thankful to all my friends and fellow hockey team members for making my stay here comfortable and an inspirational one.

A Y Santosh

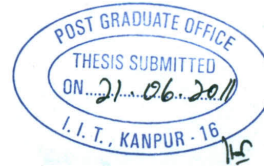
June, 2011

Abstract

The behaviour of a composite material under external loads is often quite different from that of an isotropic material. Modeling of damage in such materials is a complex problem because of the existence of several failure mechanisms at various length scales, e.g., fiber breakage, fiber-matrix debond, matrix cracks and delaminations. This poses a need for understanding the damage mechanics thoroughly at various length scales. Hence, it is impossible to create a generalized damage model by simply observing the macro-level behaviour of the composite laminate. So, the analysis of composites needs to be a multi-scale one, where, the effective field variables at each scale are obtained from the homogenization of the field variables defined at a lower scale.

Several damage models have been proposed in literature for characterization of the influence of damage modes by matrix cracks. One such generalized continuum damage model¹ is studied in the present work for transverse(normal) matrix cracks. The above model had obtained the micro level stress concentration regions which were the potential trigger points for the matrix cracks. In the present study, two independent, orthogonal, normal matrix cracks are introduced, in order to better simulate the actual physics of matrix cracking. The present matrix crack model will be compared with that proposed¹. The comparison will be done for both the material degradation model and the damage evolution models. The effect of size and mode of damage on the effective properties is also studied and definitive conclusions are drawn. The dependency of these effects on the volume fraction is also studied.

¹V. Murari, "*Micromechanics Based Continuum Damage Model for Ply Failure in Unidirectional Composites*", PhD Thesis, 2010

CERTIFICATE

It is certified that the work contained in this thesis entitled “**A homogenization based continuum damage model for transverse matrix cracks in composites**” by **Mr. A. Y. Santosh (Roll No. Y9101001)** has been carried out under my supervision and this work has not been submitted elsewhere for a degree.

Upadhyay
Dr. C. S. UPADHYAY

June, 2011

Professor

Department of Aerospace Engineering
Indian Institute of Technology Kanpur
Kanpur-208016, India

Contents

1	Introduction	1
1.1	Introduction	1
1.2	Damage Models	5
1.2.1	Damage Meso-model for Laminates (DML)	6
1.2.2	Micromechanics Based Continuum Damage Model [4] for Ply Failure in Unidirectional Composites	7
1.3	The Concept of Homogenization	10
1.4	Present Study	12
1.5	Outline of the thesis	14
2	Mathematical Theory of Homogenization	16
2.1	Introduction	16
2.2	Formulation	17
2.2.1	Effective Stiffness	23
2.2.2	Effective coefficient of thermal expansion	25
2.2.3	Effective shrinkage coefficient	27

2.2.4	Strain concentration factors and state of stress (and strain) at micro level	29
3	Models for Macro Influence of Damage	31
3.1	Micromechanics on unit-cell RVE	31
3.2	Effects of transverse matrix cracks under study on the effective properties at reference volume fraction($v_f=0.608$)	34
3.3	Free energy density function	36
4	Model Identification and Predictions	47
4.1	Model Identification	47
4.1.1	Determination of c_1	48
4.1.2	Determination of c_2	49
4.2	Model Predictions	50
5	Conclusions	69
5.1	Conclusions	69
5.2	Future scope	70

List of Figures

1.1	Commonly observed damage modes	3
1.2	Progressive Failure [13]	4
1.3	Matrix cracks considered in the present study	5
1.4	Length scales used to study composite material response	6
1.5	A hypothetical periodic domain	10
1.6	RVE smeared out into equivalent homogeneous material	11
1.7	Concentration zones and matrix cracking models	13
1.8	A z-direction matrix crack model, meshed in HyperMesh v8.0SR1	15
2.1	(a) Material with microstructure in macro scale(x_1, x_2, x_3) showing characteristic length(L) at macro scale and the characteristic length of the microstructure (ϵ). (b) Unit-cell RVE for the microstructure in fast coordinates (y_1, y_2, y_3)	18
3.1	a.) Matrix crack mc-ydr and b.) Matrix crack mc-zdr	34
3.2	Elastic properties of <i>carbon/epoxy</i> composite with <i>mc - ydr</i> ; $\Delta v_f = 0$: Comparison of homogenization and detailed models	39

3.3	Elastic properties of <i>carbon/epoxy</i> composite with $mc - ydr$; $\Delta v_f = -105$: Comparison of homogenization and detailed models	40
3.4	Elastic properties of <i>carbon/epoxy</i> composite with $mc - zdr$; $\Delta v_f = 0$: Comparison of homogenization and detailed models	41
3.5	Elastic properties of <i>carbon/epoxy</i> composite with $mc - zdr$; $\Delta v_f = -105$: Comparison of homogenization and detailed models	42
3.6	Elastic properties of <i>glass/epoxy</i> composite with $mc - ydr$; $\Delta v_f = 0$: Com- parison of homogenization and detailed models	43
3.7	Elastic properties of <i>glass/epoxy</i> composite with $mc - ydr$; $\Delta v_f = -105$: Comparison of homogenization and detailed models	44
3.8	Elastic properties of <i>glass/epoxy</i> composite with $mc - zdr$; $\Delta v_f = 0$: Com- parison of homogenization and detailed models	45
3.9	Elastic properties of <i>glass/epoxy</i> composite with $mc - zdr$; $\Delta v_f = -105$: Comparison of homogenization and detailed models	46
4.2	Prediction of tensile response of $[\pm 45]_s$ T300/914 carbon/epoxy laminates .	54
4.4	Prediction of lamina shear response of $[\pm 45]_s$ T300/914 carbon/epoxy lam- inates	55
4.6	Growth of damage parameters in a lamina of $[\pm 45]_s$ T300/914 carbon/epoxy laminates	56
4.8	Prediction of lamina tensile response of $[\pm 67.5]_s$ T300/914 carbon/epoxy laminates	57
4.10	Prediction of lamina shear response of $[\pm 67.5]_s$ T300/914 carbon/epoxy laminates	58

4.12	Growth of damage parameters in a lamina of $[\pm 67.5]_s$ T300/914 carbon/epoxy laminates	59
4.14	Prediction of tensile response of $[0/90]_s$ T300/914 carbon/epoxy laminates .	60
4.16	Growth of damage parameters in a 0^0 lamina of $[0/90]_s$ T300/914 carbon/epoxy laminates	61
4.18	Growth of damage parameters in a 90^0 lamina of $[0/90]_s$ T300/914 carbon/epoxy laminates	62
4.20	Prediction of tensile response of $[-12/78]_{2s}$ T300/914 carbon/epoxy laminates	63
4.22	Growth of damage parameters in a -12^0 lamina of $[-12/78]_{2s}$ T300/914 carbon/epoxy laminates	64
4.24	Growth of damage parameters in a 78^0 lamina of $[-12/78]_{2s}$ T300/914 carbon/epoxy laminates	65
4.26	Prediction of tensile response of $[67.5/22.5]_{2s}$ T300/914 ca/ep laminates . .	66
4.28	Growth of damage parameters in a 67.5^0 lamina of $[67.5/22.5]_{2s}$ T300/914 ca/ep laminates	67
4.30	Growth of damage parameters in a 22.5^0 lamina of $[67.5/22.5]_{2s}$ T300/914 ca/ep laminates	68

List of Tables

3.1	Least square quadratic fit data values (j_1 and j_2) corresponding to carbon/epoxy and glass/epoxy composites.	36
3.2	Least square quadratic fit data values (k_1 , k_2 and p) corresponding to matrix crack ($mc - ydr$) for carbon/epoxy and glass/epoxy composites.	37
3.3	Least square quadratic fit data values (k_1 , k_2 and p) corresponding to matrix crack ($mc - zdr$) for carbon/epoxy and glass/epoxy composites.	38
4.1	Initiation parameters of the model	47
4.2	Evolution parameters of the model	50
4.3	Differences in the lamina properties used in the model from the experiment	51

Chapter 1

Introduction

1.1 Introduction

The use of composite materials in cyclic load carrying structural members has raised questions of their durability. Recent investigations into the fatigue and fracture of composites has attracted considerable interest due to the increasing use of these materials in aerospace structures. These materials exhibit complex modes of failure both under static and fatigue loadings.

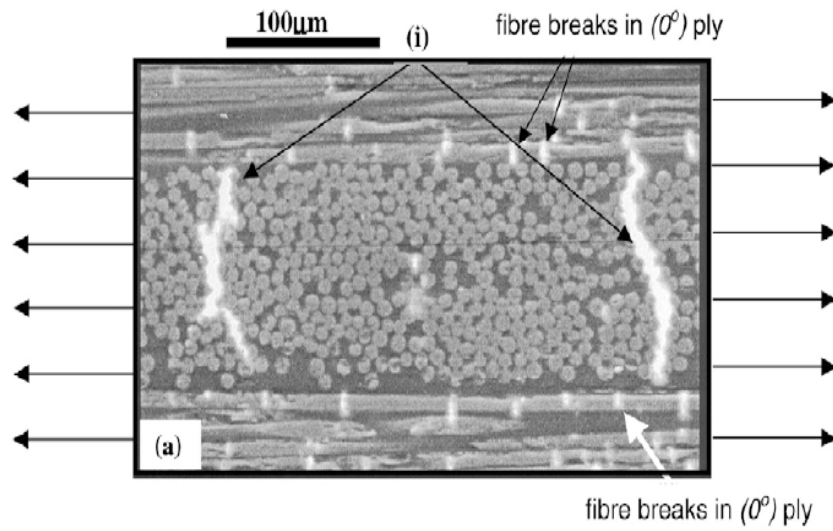
Composites are intrinsically different from metals and require a different approach to damage analysis. The key differences between metals and fiber-reinforced composites drive physically different load responses. Composites have multiple constituents with unique material properties contributing separately to the load response, so the composite stress and the constituent stress are not the same. This is where the role of multiple scales becomes important. Composite behaviour is directionally dependent as it is influenced by the orientation of the fibers and surrounding laminae. Most of the damage in composites is accumulated as microcracks in the matrix material.

This results in characteristically different responses to cyclic loading. Failure is accompanied by one or more of the following phenomena: fiber breakage (figure 1.1(a)); fiber-matrix debond (figure 1.1(b)); matrix cracking (figure 1.1(c)) and delaminations (figure 1.1(d)) and (figure 1.1(e)). These phenomena must be taken into consideration in predicting failure of the laminates. This fundamental difference in material response requires a different approach to be used for the analysis of composite damage.

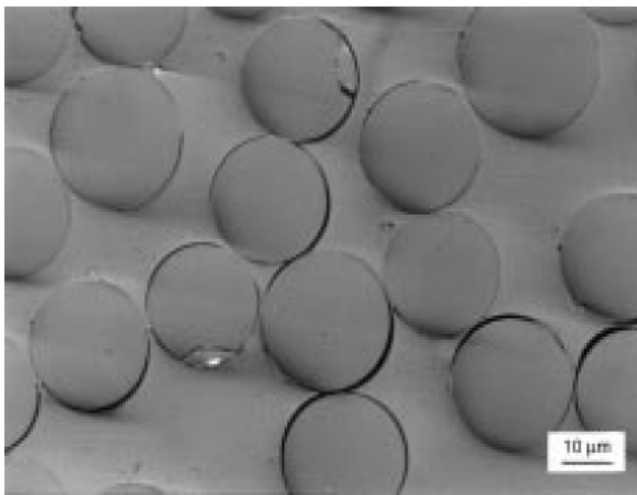
Damage in composites is different from that in metals. Metal failure is characterised by slow crack propagation; cracks initiate and propagate in a series of notch blunting and crack propagation events. By contrast, composite failure (figure (1.2)) is a progressive accumulation of damage , including multiple damage modes and complex failure mechanisms.

Prediction of micro-mechanical failure modes necessitates consideration at even smaller scale as failure of a structure is generally initiated at the locations where stress concentration is high. The current study focuses on matrix cracks (figure 1.3) in unidirectional fiber composite laminates with thermosetting matrix. The length scale of the constituents of the lamina is much smaller than the length scale of the lamina. Therefore, a representative volume element (RVE) is used, for the analysis purpose, with the assumption that the lamina can be formed by using the RVE as the basic building block. Three length scales (figure 1.4) that can be defined in the composites are: 1) Macroscale (length scale of the laminate); 2) Mesoscale (length scale of the lamina); and 3) Microscale (length scale of the RVE).

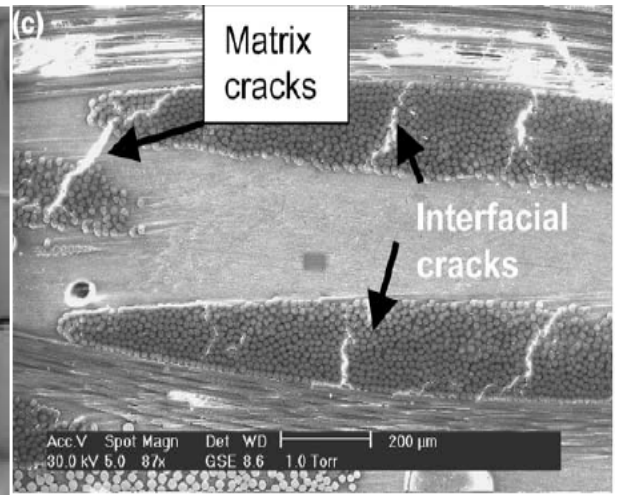
The responses of a composite at macroscale is the manifestation of the responses at the mesoscale, which in turn is the manifestation of what happens at the microscale [5]-[8]. Further, composites are increasingly used in advanced light-weight structures, especially modern aircraft structures that are mostly subjected to cyclic loads. These can lead to progressive growth and interaction of several damage mechanisms that occur at different scales, till the failure of the component. Hence, there is a need to understand the



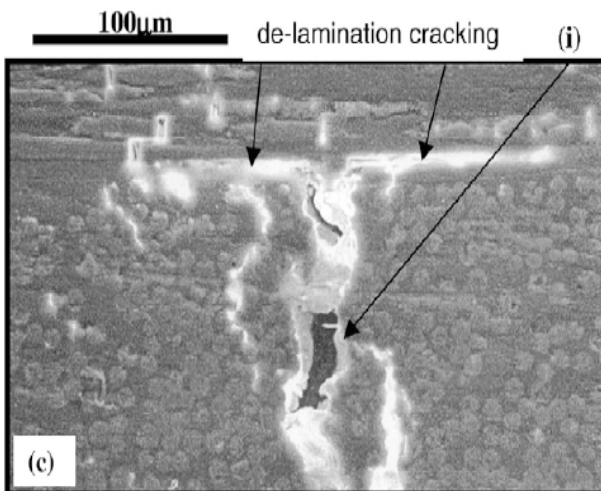
(a) Fiber breakage [14]



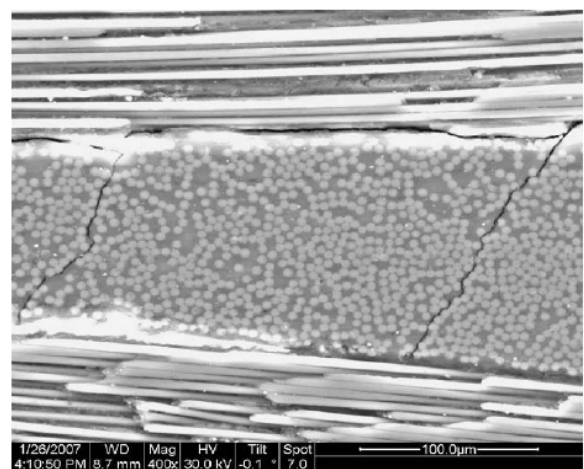
(b) Fiber-matrix debond [13]



(c) Matrix cracks [15]



(d) Delamination [14]



(e) Transverse matrix cracks with delamination [12]

Figure 1.1: Commonly observed damage modes



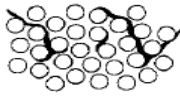




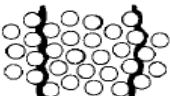
Polyester	Vinylester
 <p>Short cracks from post-curing</p>	 <p>No visual cracks</p>
 <p>Linking of cracks</p>	 <p>Debonding</p>
 <p>Complete transverse cracks</p>	 <p>Debond opening and formation of short cracks</p>
 <p>Transverse cracks + small diffuse cracks</p>	 <p>Distinct transverse cracks</p>

Figure 1.2: Progressive Failure [13]

mechanisms at different scales to develop meaningful damage models.

Further, analysis of composite requires a multiscale analysis with appropriately established connections between different scales. The process of obtaining the fields at a higher scale, based on the fields at the lower scale is termed as homogenization [9] and the process of obtaining the fields at a lower scale, from the fields at the higher scale is termed as localisation.

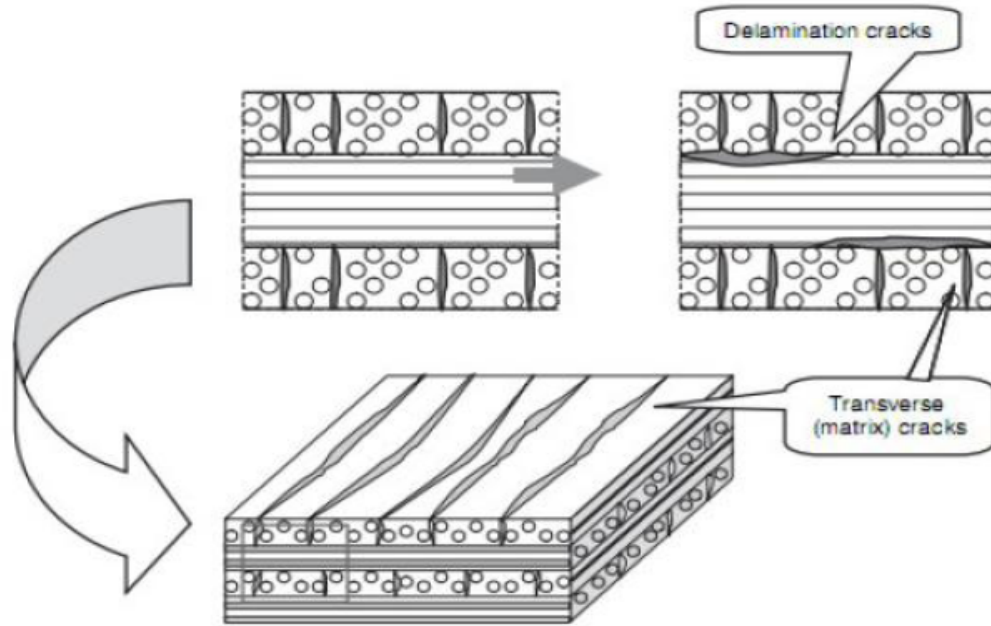


Figure 1.3: Matrix cracks considered in the present study

1.2 Damage Models

The study of initiation and accumulation of damage up to and including rupture is called *Damage Mechanics* [16]. Several growth models have been proposed in the literature, starting from the first ply failure theory, progressive ply failure theory, and others (for example the world wide failure exercise [19]). A major problem with these models is that they could predict either the initiation of damage or provide a crude global model for ply-wise damage. These models could not predict the point-wise distribution of damage or its evolution. A major problem with the existing damage mechanics based models is that the stiffness properties become zero as the damage reaches its critical value ($d_i = 1$). This leads to a material singularity at a point, where the stiffness values become zero. Thus a cut-off damage value is often employed in the evolution model to prevent the stiffness values from becoming zero. To properly estimate the amount of damage or damage accumulation, it is necessary to formulate the damage phenomenon in terms of measurable mechanical variables.

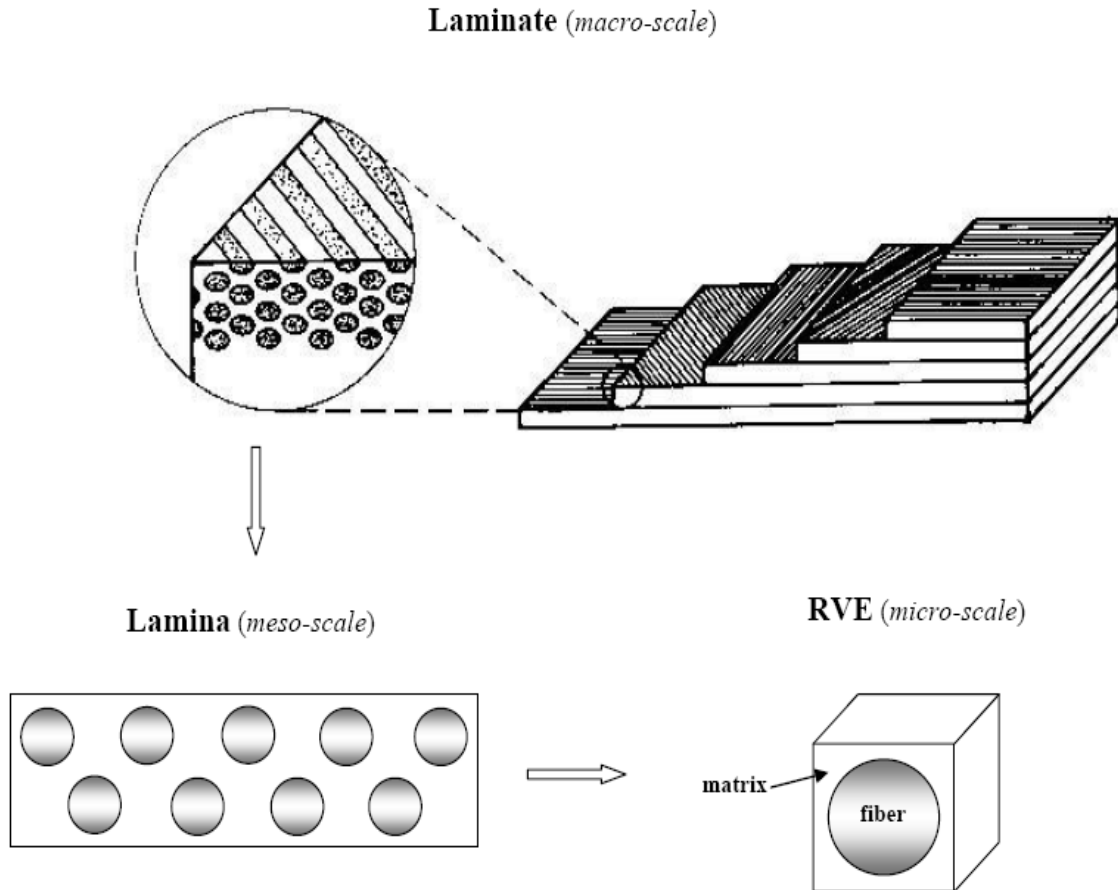


Figure 1.4: Length scales used to study composite material response

1.2.1 Damage Meso-model for Laminates (DML)

As a prelude to the existing model, a damage model proposed by Ladeveze[17] is studied, that has its foundations in irreversible thermodynamics, named *Damage Meso – model for Laminates* (DML). This model is an example for meso-macro approach. A bridge between the micro and meso level is presented in [20]. However, the link between the micro-meso is not clear. This meso-model is based on the hypothesis that the behavior of any laminate can be described using elementary entities called *meso constituents*. These are the ply and the interfacial layers that lie in between two plies (or laminae). It is assumed that the response of the laminate (of any stacking sequence), subjected to any loading, can be obtained once the behavior of the meso constituents is identified. The

response of a damaged layer at any instant of time (or loading conditions) is expressed in terms of degradation in the stiffness properties and the build-up of inelastic strains due to damage and/or matrix plasticity. This theory has been shown to be both accurate and versatile for application to a wide variety of fibrous composite laminates. The damage model uses three damage variables, one for fiber breakage and other two are matrix modes representing fibre-matrix debonding and transverse matrix cracking. The damage evolution law is based on the experimental observations of the response of a damaged layer.

1.2.2 Micromechanics Based Continuum Damage Model [4] for Ply Failure in Unidirectional Composites

In light of the above discussion, the studied model [4] focuses on developing a detailed micromechanical analysis at the level of the constituents (fiber and matrix) in order to understand the local state of stresses and strains. Damage mechanisms are identified based on these stresses (and strains) and the damage parameters are characterized in terms of damage sizes of these damage mechanisms at the micro level. Based on the literature and available experimental evidence, the micro-level damage mechanisms identified are: 1) Fiber breakage, 2) fiber-matrix debond, and 3) matrix cracks. The micromechanical analysis is done, using the mathematical theory of homogenisation, on a representative volume element (RVE) with and without damage.

The study also systematically brings in the effects of volume fraction, which is normally ignored in the study of damage in the literature. Further, the study focuses on implementing a simple model for residual stresses developed due to cure process. The model is based on cooling down of completely cured composites from cure temperature to room temperature. The model assumes that the curing is complete before cooling down process and there is no change in the elastic properties during the cooling down process. Based on the study of residual stresses, a detailed model is developed for the degradation

of the coefficient of thermal expansion in terms of damage. This brings out a very important feature which is often missed in the damage modeling - that of the additional residual strains being generated due to damage (which can be linked to the thermal cure induced strains).

Using arguments from continuum thermodynamics and necessary consistency condition on the dissipation of energy, a simplified model for evolution of damage is developed in this study. This forms the framework for obtaining the evolution equation for the damage variables. The evolution model is defined in terms of the macro-stresses, but is based on the micromechanical observations and thought experiments. The parameters in the evolution model are obtained from the available data from experiments conducted on the selected composite laminates. The damage initiation criteria is also defined in terms of macrostresses, but is based on stress concentration factors in the critical regions, identified from the micromechanical analysis.

The restriction imposed by the second law of thermodynamics is given by equation (1.2.1), which is repeated here for the sake of completeness.

$$A_i \dot{d}_i + \sigma_{ij} \dot{e}_{ij}^R \geq 0 \quad (1.2.1)$$

Note that, A_i can be understood as the energy release rate associated with the assumed damage mode. Hence, the first term in equation (1.2.1) leads to dissipation of energy due to growth of the damage. So, by definition A_i is positive by itself. Therefore, the term, $A_i \dot{d}_i$, is used for modeling damage evolution with this understanding. The second part of equation (1.2.1) will be due to two factors: 1) Matrix plasticity, \dot{e}_{ij} . 2) Effect of damage on initial state of stress, $e_{ij}^{d,R}$. Since this is a micromechanical analysis, it is attempted to create a simple model to understand the cause for this plastic behavior at macro level. It will be shown that this is due to the characteristics of the matrix, which is modeled through a simplified elastic-perfectly plastic model. Thus, the second part of

equation (1.2.1) will be modeled through a simplified model of a hardening material at the macroscopic level and is presented in the subsequent chapter. The only restriction on the evolution model is found out to be

$$\dot{d}_i \geq 0 \quad (1.2.2)$$

Based on the obtained condition (1.2.2) the following evolution laws were obtained:

Fiber breakage: Despite the fact that the fiber breakage is an instantaneous event, a smooth evolution model was proposed as follows.

$$d_1 = 0; \text{ when, } \sigma_{11} \leq \Lambda \sigma_{11}^f \quad (1.2.3)$$

$$d_1 = \max_{\tau \leq t} \frac{\sigma_{11} - \Lambda \sigma_{11}^f}{(1 - \Lambda) \sigma_{11}^f}; \text{ when, } \sigma_{11} \geq \Lambda \sigma_{11}^f \quad (1.2.4)$$

where τ denotes any time (or load step) previous to the current time (or load step) t ; σ_{11}^f is the failure stress for the fiber; Λ is chosen such that the damage initiates very close to the failure stress. Here, Λ is chosen as 0.8.

Fiber/matrix debond: The evolution model for the fiber-matrix debond is given as

$$d_2 = 0; \text{ when, } |\sigma_{12}| \leq |\sigma_{12}^c| \quad (1.2.5)$$

$$d_2 = c_1 \max_{\tau \leq t} \langle |\sigma_{12}| - |\sigma_{12}^c| \rangle_+; \text{ when, } |\sigma_{12}| \geq |\sigma_{12}^c| \quad (1.2.6)$$

where σ_{12}^c is the critical stress at which the fiber-matrix debond initiates. Note that it is assumed here that growth of d_2 is independent of sign of σ_{12} .

Matrix cracks: The evolution model for the matrix crack is given as

$$d_3 = 0; \text{ when, } \sigma_{22} \leq \sigma_{22}^c \quad (1.2.7)$$

$$d_3 = c_2 \max_{\tau \leq t} \langle \sigma_{22} - \sigma_{22}^c \rangle_+; \text{ when, } \sigma_{22} > \sigma_{22}^c \quad (1.2.8)$$

where σ_{22}^c is the critical stress at which the matrix crack initiates and the $\langle \cdot \rangle$ denotes the positive part.

1.3 The Concept of Homogenization

Composite materials generally comprise of a domain with locally periodic structure which arises from the assembly of different heterogeneous media with different material behaviour. The domain can be idealized to be formed of periodically repeating cells of the type shown in (figure 1.5). Note that, however, , these periodically repeating cells are never intact at the boundaries due to rough finishing of the composite fabric. To demonstrate the concept of homogenization, let us consider the locally periodic domain Ω shown in (figure 1.5), subjected to the traction vector T_j for $j = 1,2,3$ on the force boundary Γ_N and subjected to displacement boundary conditions on Γ_D . Let $\partial\Omega = \Gamma_N \cup \Gamma_D$.

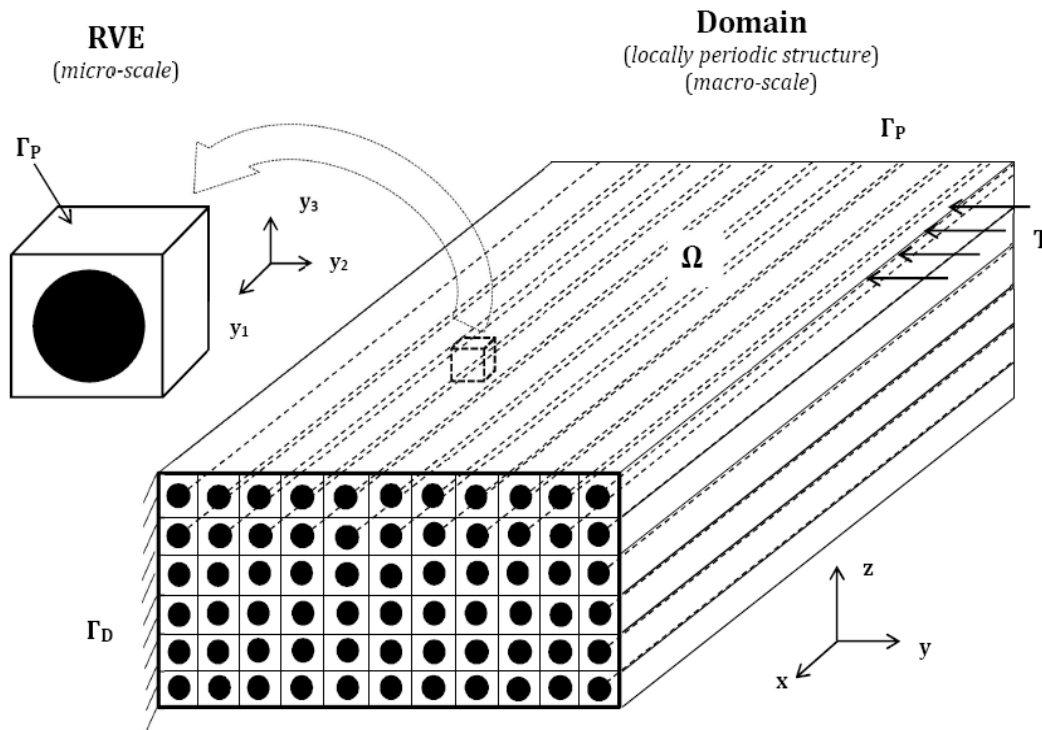


Figure 1.5: A hypothetical periodic domain

The complete domain Ω is built up of the repeating units called RVEs (representative volume elements). Each RVE comprises of a fiber part and a matrix which holds together the fiber. Use of fiber embedded in surrounding matrix leads to discontinuity in the material properties. The task of obtaining a numerical solution to this problem is

computationally complex as the mesh has to be very fine over each RVE so as to capture the full material detail. Now, this leads to a massive matrix problem which may be computationally difficult to solve. In order to overcome such bottlenecks during computation and get a good approximate solution to the problem, several averaging methods have been proposed. Mathematical theory of homogenization [9] has been used as one of the primary tools in recent past for analyzing the heterogeneous composite media. The theory says that in periodic heterogeneous media like the composites, the solution can be broken down into two components viz. the micro-level (oscillatory) part which is smeared and superimposed on a macro-level (smooth) part. In this method micro level problems are solved to obtain the mechanics at the macro scale, the resulting equations are called homogenized or averaged equations and the coefficients associated with them are called *homogenized* or *effective* coefficients (figure 1.6).

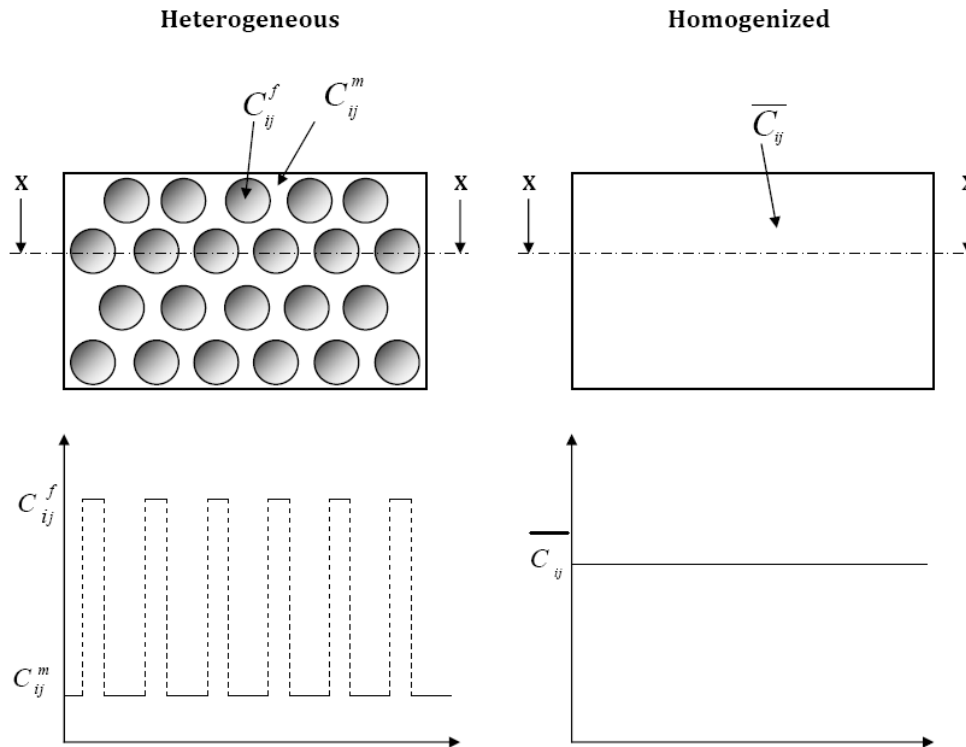


Figure 1.6: RVE smeared out into equivalent homogeneous material

1.4 Present Study

The existing damage model [4] developed had come up with certain regions of concentration zones (figure 1.7(a)) inside the RVE under external loading. These high stress level zones are potential regions for the matrix cracks to initiate. Once the matrix cracks are initiated the direction of their growth can be in either of the two directions shown (figure 1.7(b)). Note that the model of [4] assumes that the matrix cracks in both directions grow symmetrically, starting from the fiber surface.

The present work is an attempt to study the matrix crack growth model which is on the right side(II) of the figure 1.7(b). This will help one understand the nature of growth law associated with this crack(II) and draw conclusions about whether the growth law is governed by the direction of matrix crack growth or is only dependent on the size of the matrix crack. In this study several numerical experiments are performed, based upon the theory of homogenization for both undamaged and damaged cases, on 3-dimensional unit-cell RVEs. The damaged RVEs are analyzed to develop the growth law. It is expected that the proposed model for matrix crack location and growth is more realistic, as it emanates from the region of stress concentration and leads to a directional dependence of stiffness on the crack. In the current study only the matrix crack oriented along the local vertical is considered, as in a laminate, the dominant stresses will be σ_{22} (and not σ_{33}). The model for matrix cracks considered in [4] is transversely isotropic, which is evident from the symmetric cracks considered. The present model for matrix cracks considered is orthotropic in nature, but transverse isotropy is assumed for modelling purposes.

The unit-celled RVE is modeled and meshed using HyperMesh, a versatile meshing tool, particularly for problems of this nature. One of the several models which were being used for the computations is shown in (figure 1.8)

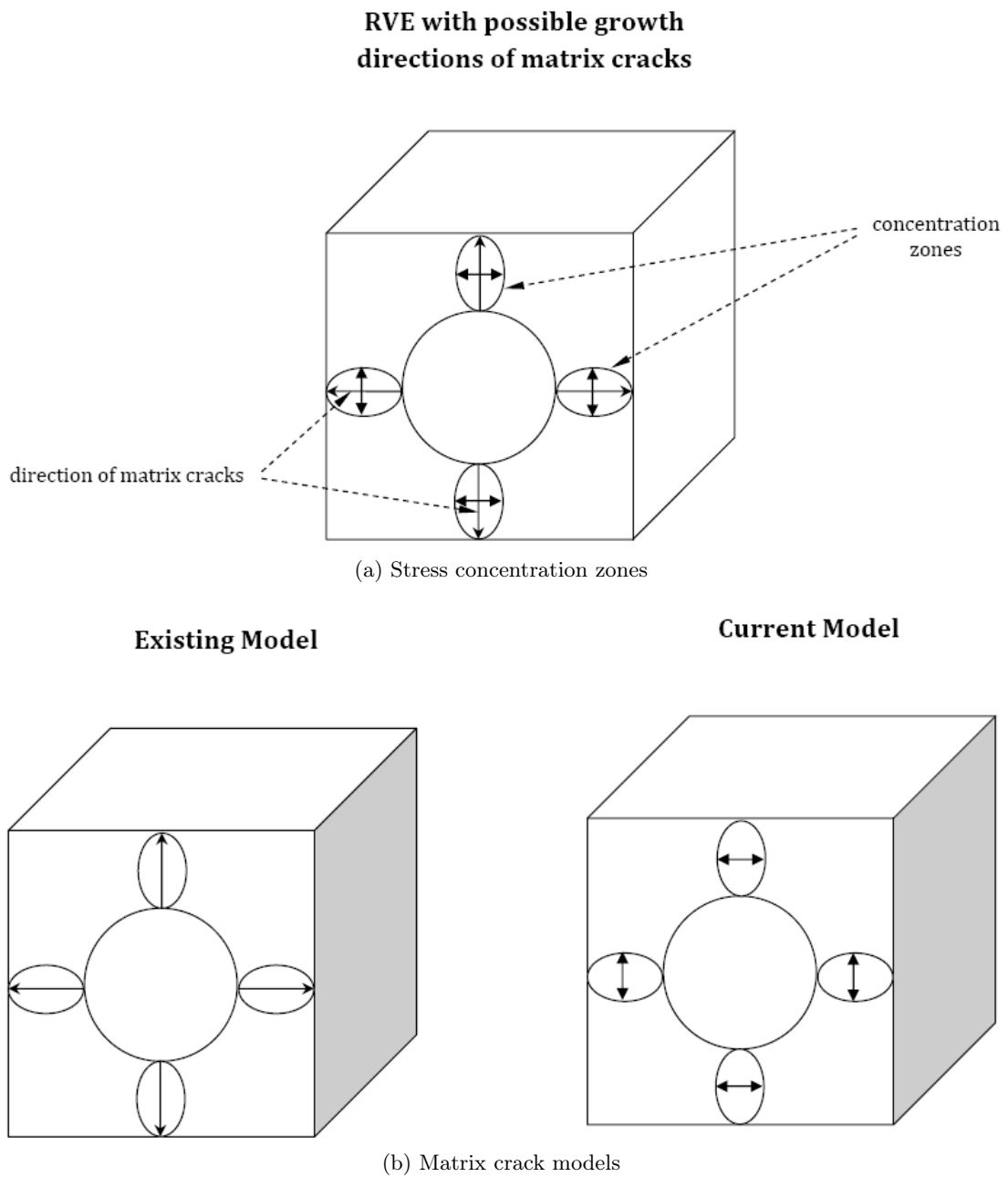


Figure 1.7: Concentration zones and matrix cracking models

1.5 Outline of the thesis

The present work is outlined as follows:

1. The first chapter introduces the importance of micromechanics and briefly gives an idea of the homogenization theory applied to periodic heterogeneous media.
2. In the next chapter a detailed formulation of the homogenization theory is presented alongside the derivation of the weak formulation.
3. The third chapter deals with the macro influence of damage and parametric studies.
4. In the fourth chapter, model identification and model predictions are presented.
5. The final chapter closes with the conclusions and suggestions for future study.

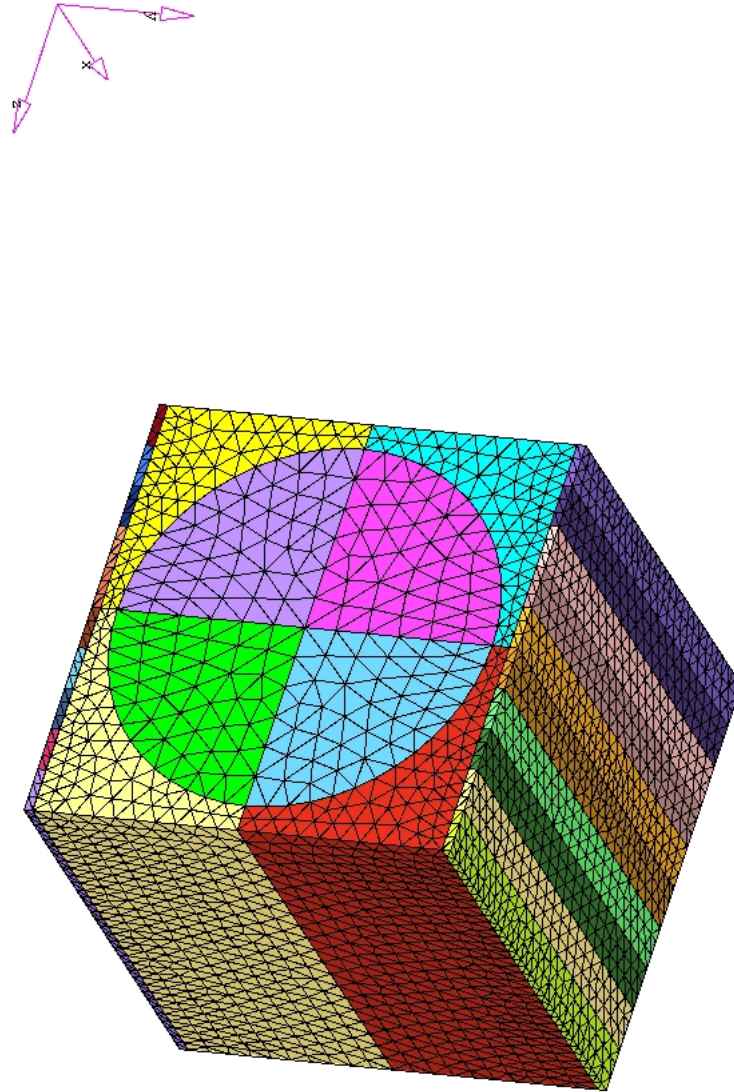


Figure 1.8: A z-direction matrix crack model, meshed in HyperMesh v8.0SR1

Chapter 2

Mathematical Theory of Homogenization

2.1 Introduction

In this chapter a mathematical tool is developed based on the *mathematical theory of homogenisation* [9]. This method is based on an asymptotic expansion over multiple scales which ensures a consistent correlation between the micro-structure and macro level responses. The formulation is mainly focused on obtaining the effective elastic properties, effective thermal and shrinkage properties and stress-strain concentration factors which help compute the micro level stress-strain distribution in fiber and matrix due to various mechanical and process induced loads.

Materials that possess microstructure can be modeled using partial differential equations with rapidly oscillating coefficients. Periodic micro level problems associated with such materials are solved to get equations with slowly oscillating coefficients at the macroscopic scale the equations so obtained are called the homogenized or averaged equations with their coefficients being termed as *homogenized* or *effective* coefficients.

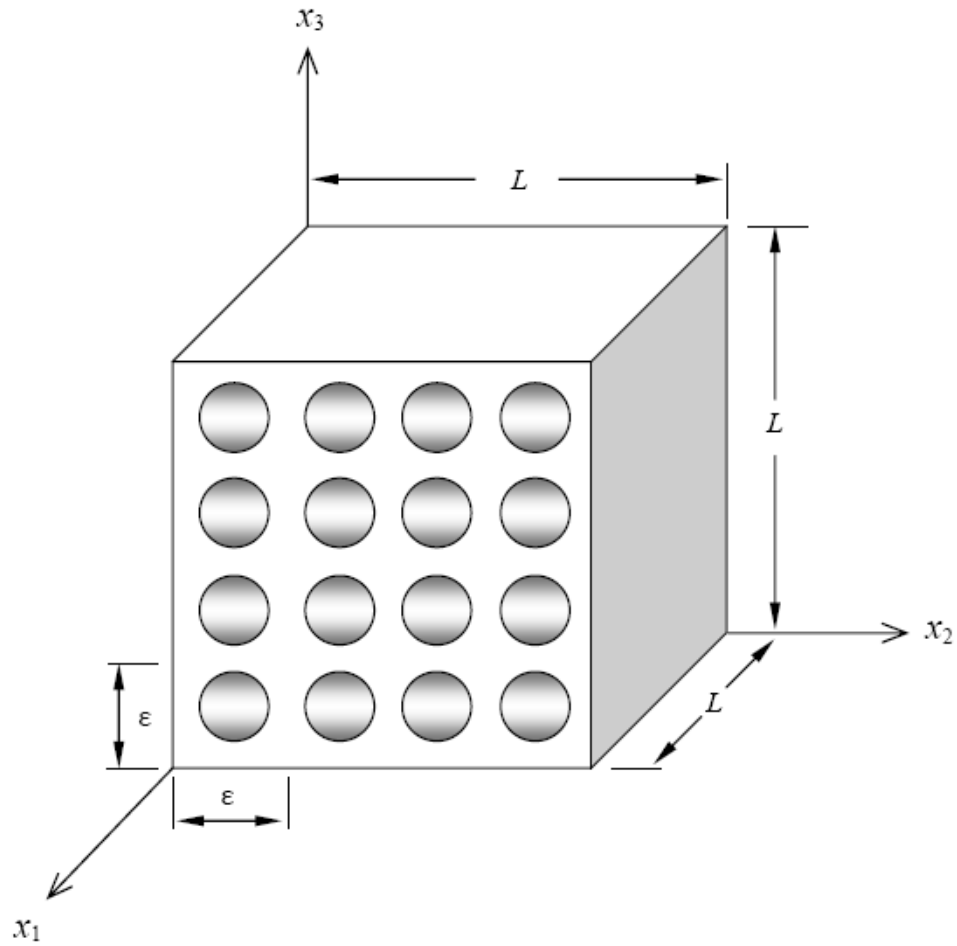
The arrangement of microstructure is assumed to be a periodically distributed square array in a thermosetting matrix like epoxy. The unit celled RVE could be chosen as shown (figure 1.5). Let the size of the unit cell be $\varepsilon \times \varepsilon \times \varepsilon$ and $\varepsilon \ll \min(L, l)$ where L is the length scale of the lamina and l is the characteristic size of the problem. For example, l is a characteristic wavelength, if the problem under consideration is the study of wave propagation.

The fast coordinate \mathbf{y} is defined in such a way that, $\mathbf{y} = \frac{\mathbf{x}}{\varepsilon}$. This coordinate is called the fast coordinate as it may be considered to vary faster, by the parameter $\frac{1}{\varepsilon}$, than the \mathbf{x} coordinate, where \mathbf{x} is called the slow coordinate [9]. In terms of these fast coordinates, the size of the unit cell becomes $1 \times 1 \times 1$. The fast coordinates correspond to the micro scale and the slow coordinates corresponds to the macro scale. All the field variables are assumed to vary on these multiple scales. The asymptotic homogenization method involves the following steps:

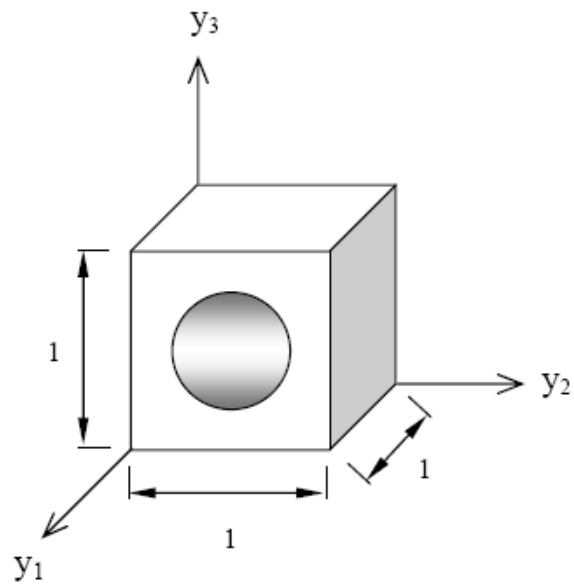
1. The solution is assumed as an asymptotic expansion in terms of the parameter ε .
2. Different powers of ε are equated, a set of equations at successive orders ε are deduced.
3. The equations obtained above with different orders are solved successively to obtain the homogeneous or averaged or macro-scale equations, effective coefficients and the concentration factors. This requires solution of micro or cell level problem.

2.2 Formulation

Consider the region Ω containing the heterogeneous material with Γ_1 and Γ_2 as the displacement and traction boundary conditions respectively. Let e_{kl} , e_{kl}^{th} , e_{kl}^{sh} , $u_i^\varepsilon = u_i(\mathbf{x}, \mathbf{y})$, f_i , t_i , and n_i be the total strain tensor, the strain tensor due to free thermal expansion, the strain tensor due to free shrinkage, the displacement field, the external force field, the surface force field and outer unit normal to the boundary of Ω , respectively. Due to the



(a)



(b)

Figure 2.1: (a) Material with microstructure in macro scale (x_1, x_2, x_3) showing characteristic length (L) at macro scale and the characteristic length of the micro structure (ϵ) . (b) Unit-cell RVE for the microstructure in fast coordinates (y_1, y_2, y_3)

repetitive constituents, the components of the stiffness tensor, C_{ijkl}^ε , the thermal expansion coefficient matrix, α_{kl}^ε , and the shrinkage coefficient matrix, η_{kl}^ε are periodic functions with a period ε .

The equilibrium state of the material (including thermal and shrinkage effects) is described by the following system of equations:

$$-\frac{\partial}{\partial x_j} \left[C_{ijkl}^\varepsilon \left(e_{kl}(\mathbf{u}^\varepsilon) - e_{kl}^{th} - e_{kl}^{sh} \right) \right] = f^\varepsilon, \quad \forall x \in \Omega \quad (2.2.1)$$

$$u_i^\varepsilon = \bar{u}_i, \quad \forall x \in \Gamma_1 \quad (2.2.2)$$

$$\sigma_{ij}^\varepsilon n_j = t_i, \quad \forall x \in \Gamma_2 \quad (2.2.3)$$

where,

$$C_{ijkl}^\varepsilon(\mathbf{x}) = \begin{cases} C_{ijkl}^f, & \text{if the point } \mathbf{x} \text{ corresponds to the fiber} \\ C_{ijkl}^m, & \text{if the point } \mathbf{x} \text{ corresponds to the matrix} \end{cases} \quad (2.2.4)$$

$$e_{kl}(\mathbf{u}^\varepsilon) = \frac{1}{2} \left(\frac{\partial u_k^\varepsilon}{\partial x_l} + \frac{\partial u_l^\varepsilon}{\partial x_k} \right) \quad (2.2.5)$$

$$e_{kl}^{th} = \alpha_{kl}^\varepsilon \Delta T, \quad \Delta T = T_c - T_r \quad (2.2.6)$$

where, T_c , T_r is the cure and the room temperature respectively

$$\alpha_{kl}^\varepsilon(\mathbf{x}) = \begin{cases} \alpha_{kl}^f, & \text{if the point } \mathbf{x} \text{ corresponds to the fiber} \\ \alpha_{kl}^m, & \text{if the point } \mathbf{x} \text{ corresponds to the matrix} \end{cases} \quad (2.2.7)$$

$$e_{kl}^{sh} = \eta_{kl}^\varepsilon \frac{\Delta V}{V} \quad (2.2.8)$$

where, $\frac{\Delta V}{V}$ is the change in volume per unit volume due to chemical shrinkage

$$\eta_{kl}^\varepsilon(\mathbf{x}) = \begin{cases} \eta_{kl}^f, & \text{if the point } \mathbf{x} \text{ corresponds to the fiber} \\ \eta_{kl}^m, & \text{if the point } \mathbf{x} \text{ corresponds to the matrix} \end{cases} \quad (2.2.9)$$

Effects of two scales is separated out by defining two coordinates: a slow coordinate, \mathbf{x} and a fast coordinate, \mathbf{y} as

$$\mathbf{x} \text{ and } \mathbf{y} = \frac{\mathbf{x}}{\varepsilon} \quad (2.2.10)$$

All the field variables are assumed to be a function of the two scales. For any function $\Phi^\varepsilon(\mathbf{x}) = \Phi(\mathbf{x}, \mathbf{y} = \frac{\mathbf{x}}{\varepsilon})$, we have (by chain rule), the following equation (2.2.11):

$$\frac{\partial \Phi^\varepsilon}{\partial \mathbf{x}} = \frac{\partial \Phi}{\partial \mathbf{x}} + \frac{1}{\varepsilon} \frac{\partial \Phi}{\partial \mathbf{y}} \quad (2.2.11)$$

By using the chain rule (2.2.11), the expression for strain (2.2.5) can be given by the following.

$$e_{kl}(\mathbf{u}^\varepsilon) = \frac{1}{2} \left(\frac{\partial u_k^\varepsilon}{\partial x_l} + \frac{\partial u_l^\varepsilon}{\partial x_k} \right) \quad \text{from (2.2.5)} \quad (2.2.12)$$

$$= \frac{1}{2} \left[\left(\frac{\partial u_k}{\partial x_l} + \frac{1}{\varepsilon} \frac{\partial u_k}{\partial y_l} \right) + \left(\frac{\partial u_l}{\partial x_k} + \frac{1}{\varepsilon} \frac{\partial u_l}{\partial y_k} \right) \right] \quad \text{by using (2.2.11)} \quad (2.2.13)$$

$$= e_{kl}^x(\mathbf{u}(\mathbf{x}, \mathbf{y})) + \frac{1}{\varepsilon} e_{kl}^y(\mathbf{u}(\mathbf{x}, \mathbf{y})) \quad (2.2.14)$$

where the operators $e_{kl}^x(\mathbf{u}(\mathbf{x}, \mathbf{y}))$ and $e_{kl}^y(\mathbf{u}(\mathbf{x}, \mathbf{y}))$ are defined as follows. For any function $\mathbf{u}^\varepsilon(\mathbf{x}) = \mathbf{u}(\mathbf{x}, \mathbf{y} = \frac{\mathbf{x}}{\varepsilon})$

$$e_{kl}^x(\mathbf{u}^\varepsilon) = \frac{1}{2} \left(\frac{\partial u_k}{\partial x_l} + \frac{\partial u_l}{\partial x_k} \right) \quad (2.2.15)$$

$$e_{kl}^y(\mathbf{u}^\varepsilon) = \frac{1}{2} \left(\frac{\partial u_k}{\partial y_l} + \frac{\partial u_l}{\partial y_k} \right) \quad (2.2.16)$$

Now, by using (2.2.14) and (2.2.11) in equation (2.2.1) and collecting the different powers of ε together, we obtain equation (2.2.17):

$$\varepsilon^{-2} A_0 \mathbf{u}^\varepsilon + \varepsilon^{-1} A_1 \mathbf{u}^\varepsilon + A_2 \mathbf{u}^\varepsilon = f_i^\varepsilon - \frac{\partial}{\partial x_j} C_{ijkl}^\varepsilon \left(\alpha_{kl}^\varepsilon \Delta T + \eta_{kl}^\varepsilon \frac{\Delta V}{V} \right) - \varepsilon^{-1} \left[\frac{\partial}{\partial y_j} C_{ijkl}^\varepsilon \left(\alpha_{kl}^\varepsilon \Delta T + \eta_{kl}^\varepsilon \frac{\Delta V}{V} \right) \right] \quad (2.2.17)$$

where, A_0 , A_1 , and A_2 are operators which are defined as follows. For any function $\Phi^\varepsilon(\mathbf{x}, \mathbf{y})$:

$$A_0\Phi^\varepsilon = -\frac{\partial}{\partial y_j} (C_{ijkl}^\varepsilon e_{kl}^y(\Phi^\varepsilon)) \quad (2.2.18)$$

$$A_1\Phi^\varepsilon = -\frac{\partial}{\partial x_j} (C_{ijkl}^\varepsilon e_{kl}^y(\Phi^\varepsilon)) - \frac{\partial}{\partial y_j} (C_{ijkl}^\varepsilon e_{kl}^x(\Phi^\varepsilon)) \quad (2.2.19)$$

$$A_2\Phi^\varepsilon = -\frac{\partial}{\partial x_j} (C_{ijkl}^\varepsilon e_{kl}^x(\Phi^\varepsilon)) \quad (2.2.20)$$

The asymptotic expansions of u_i^ε and f_i^ε are defined as follows (equations (2.2.21) and (2.2.22)).

$$u_i^\varepsilon(\mathbf{x}) = u_i(\mathbf{x}, \mathbf{y}) = u_i^{(0)}(\mathbf{x}, \mathbf{y}) + \varepsilon u_i^{(1)}(\mathbf{x}, \mathbf{y}) + \varepsilon^2 u_i^{(2)}(\mathbf{x}, \mathbf{y}) + \dots \quad (2.2.21)$$

$$f_i^\varepsilon(\mathbf{x}) = f_i(\mathbf{x}, \mathbf{y}) = f_i^{(0)}(\mathbf{x}, \mathbf{y}) + \varepsilon f_i^{(1)}(\mathbf{x}, \mathbf{y}) + \varepsilon^2 f_i^{(2)}(\mathbf{x}, \mathbf{y}) + \dots \quad (2.2.22)$$

where $u_i^{(n)}$ and $f_i^{(n)}$, $n = 0, 1, 2, \dots$ are y -periodic.

By using equation (2.2.21) and the fact that different powers of ε are independent of each other, in equation (2.2.17), the following equations are obtained.

$$A_0\mathbf{u}^{(0)} = 0 \quad (2.2.23)$$

$$A_0\mathbf{u}^{(1)} + A_1\mathbf{u}^{(0)} = -\frac{\partial}{\partial y_j} C_{ijkl}^\varepsilon \left(\alpha_{kl}^\varepsilon \Delta T + \eta_{kl}^\varepsilon \frac{\Delta V}{V} \right) \quad (2.2.24)$$

$$A_0\mathbf{u}^{(2)} + A_1\mathbf{u}^{(1)} + A_2\mathbf{u}^{(0)} = f_i^{(0)}(\mathbf{x}, \mathbf{y}) - \frac{\partial}{\partial x_j} C_{ijkl}^\varepsilon \left(\alpha_{kl}^\varepsilon \Delta T + \eta_{kl}^\varepsilon \frac{\Delta V}{V} \right) \quad (2.2.25)$$

The following lemma is used in solving the equations (2.2.23) to (2.2.25), see [9] for details.

Lemma 1. Let $C_{ijkl}(\mathbf{y})$, $\Phi(\mathbf{y})$ and $F(\mathbf{y})$ be y -periodic. Then a necessary and sufficient condition for a y -periodic solution of the equation

$$A_0\Phi \equiv -\frac{\partial}{\partial y_j} (C_{ijkl}^\varepsilon e_{kl}^y(\Phi)) = F(\mathbf{y}) \quad (2.2.26)$$

to exist is the following.

$$\langle F \rangle = \frac{1}{|Y|} \int_Y F(\mathbf{y}) d\mathbf{y} = 0 \quad (2.2.27)$$

If a \mathbf{y} -periodic solution Φ exists, then it is unique up to a constant vector C . The general \mathbf{y} -periodic solution of equation (2.2.26) can be written as $\Phi(\mathbf{y}) = \bar{\Phi}(\mathbf{y}) + C$, where $\bar{\Phi}(\mathbf{y})$ is a solution of (2.2.26) with zero mean over the period: $\langle \bar{\Phi} \rangle = 0$, C is an arbitrary constant vector.

Remark. *The integral in the above equation represents the summation of piecewise integrals in the fiber and the matrix domain.*

SOLUTION OF EQUATION (2.2.23):

By virtue of equations (2.2.26) and (2.2.27), the only periodic solution of (2.2.23) is $\mathbf{u}^{(0)} = \text{constant}$ where \mathbf{x} is a parameter, i.e.

$$\mathbf{u}^{(0)}(\mathbf{x}, \mathbf{y}) = \mathbf{v}^{(0)}(\mathbf{x}) \quad (2.2.28)$$

SOLUTION OF EQUATION (2.2.24):

Using (2.2.28), (2.2.24) reduces to

$$A_0 \mathbf{u}^{(1)} = \frac{\partial}{\partial y_j} C_{ijkl}(\mathbf{y}) \left(e_{kl}^x(\mathbf{v}_0) - \alpha_{kl}^\varepsilon \Delta T - \eta_{kl}^\varepsilon \frac{\Delta V}{V} \right) \quad (2.2.29)$$

In (2.2.29) the parentheses collectively represents mechanical strains and individually they correspond to the total, thermal and shrinkage strain. Further, ΔT , $\frac{\Delta V}{V}$ and $e_{kl}^x(\mathbf{v}_0)$ are functions of slow variable \mathbf{x} only. \mathbf{x} is just a parameter and the equation may be regarded as a problem depending on the variable \mathbf{y} only. Therefore, the solution exists by virtue of equations (2.2.26) and (2.2.27). In order to obtain the effective properties and the micro-stresses the solution of equation (2.2.29) is necessary. The determination of effective stiffness, strain concentration factors, effective coefficient of thermal expansion, effective

coefficient of shrinkage, and the state of micro-stresses are described in the following subsections.

2.2.1 Effective Stiffness

The effective stiffness and the strain concentration factors are obtained using the equations (2.2.29) with $\Delta T = 0$ and $\frac{\Delta V}{V} = 0$. The general solution of the resulting equation may be assumed in the following form (equation (2.2.30)):

$$\mathbf{u}^{(1)}(\mathbf{x}, \mathbf{y}) = \boldsymbol{\chi}^{rs} e_{rs}^x(\mathbf{v}_0(\mathbf{x})) + \mathbf{w}_1(\mathbf{x}) \quad (2.2.30)$$

Note that the expression above means that the micro solution is written as a combination of solutions corresponding to individual macro-strains e_{rs}^x . Substituting $\mathbf{u}^{(1)}$ in (2.2.29), with $\Delta T = 0$ and $\frac{\Delta V}{V} = 0$, yields,

$$A_0 \{ \boldsymbol{\chi}^{rs} e_{rs}^x(\mathbf{v}_0(\mathbf{x})) + \mathbf{w}_1(\mathbf{x}) \} = \left\{ \frac{\partial}{\partial y_j} C_{ijkl}(\mathbf{y}) \right\} e_{kl}^x(\mathbf{v}_0) \quad (2.2.31)$$

$$A_0 \{ \boldsymbol{\chi}^{rs} e_{rs}^x(\mathbf{v}_0(\mathbf{x})) \} = \left\{ \frac{\partial}{\partial y_j} C_{ijkl}(\mathbf{y}) \right\} e_{kl}^x(\mathbf{v}_0) \quad (2.2.32)$$

$$\left\{ A_0 \boldsymbol{\chi}^{rs} - \frac{\partial}{\partial y_j} C_{ijrs}(\mathbf{y}) \right\} e_{rs}^x(\mathbf{v}_0(\mathbf{x})) = 0 \quad (2.2.33)$$

By equation (2.2.33), it suffices to consider the following auxiliary problem.

$$A_0 \boldsymbol{\chi}^{rs} = \frac{\partial}{\partial y_j} (C_{ijrs}(\mathbf{y})), \boldsymbol{\chi}^{rs} \text{ is } y\text{-periodic} \quad (2.2.34)$$

The above problem is solved over unit-cell RVE by using finite element method.

SOLUTION OF EQUATION (2.2.25):

When $\mathbf{u}^{(0)}$ and $\mathbf{u}^{(1)}$ are known, the equation (2.2.25) with $\Delta T = 0$ and $\frac{\Delta V}{V} = 0$, can be written as:

$$A_0 \mathbf{u}^{(2)} = f^{(0)} - A_1 \mathbf{u}^{(1)} - A_2 \mathbf{u}^{(0)} \quad (2.2.35)$$

By virtue of the equations (2.2.26) and (2.2.27), y-periodic solution $\mathbf{u}^{(2)}$ exists if and only if

$$\langle f^{(0)} - A_1 \mathbf{u}^{(1)} - A_2 \mathbf{u}^{(0)} \rangle = 0 \quad (2.2.36)$$

Substituting for $\mathbf{u}^{(0)}$ and $\mathbf{u}^{(1)}$ from (2.2.28) and (2.2.30), the condition (2.2.36) yields

$$\begin{aligned} \int_Y \left\{ f^{(0)} + \frac{\partial}{\partial x_j} ([C_{ijrs}^\varepsilon + C_{ijkl}^\varepsilon e_{kl}^y(\boldsymbol{\chi}^{rs})] e_{rs}^x(\mathbf{v}_0)) + \right. \\ \left. + \frac{1}{2} \frac{\partial}{\partial y_j} (C_{ijkl}^\varepsilon \boldsymbol{\chi}_k^{rs}) \frac{\partial}{\partial x_l} (e_{rs}^x(\mathbf{v}_0)) + \frac{1}{2} \frac{\partial}{\partial y_j} (C_{ijkl}^\varepsilon \boldsymbol{\chi}_l^{rs}) \frac{\partial}{\partial x_k} (e_{rs}^x(\mathbf{v}_0)) + \right. \\ \left. + e_{kl}^x(\mathbf{w}_1) \frac{\partial}{\partial y_j} (C_{ijkl}^\varepsilon) \right\} dy = 0 \end{aligned} \quad (2.2.37)$$

The functions C_{ijkl} and $\boldsymbol{\chi}^{rs}$ are y-periodic and the functions $e_{kl}^x(\mathbf{w}_1)$, $\frac{\partial}{\partial x_i} (e_{rs}^x(\mathbf{v}_0))$ and $\frac{\partial}{\partial x_k} (e_{rs}^x(\mathbf{v}_0))$ are independent of \mathbf{y} . Therefore, by Gauss divergence theorem, the third, fourth and fifth terms of equation (2.2.37) vanish yielding the following.

$$\int_Y f^{(0)} dy + \frac{\partial}{\partial x_j} \left(\left\{ \int_Y [C_{ijrs}^\varepsilon + C_{ijkl}^\varepsilon e_{kl}^y(\boldsymbol{\chi}^{rs})] dy \right\} e_{rs}^x(\mathbf{v}_0) \right) = 0 \quad (2.2.38)$$

or

$$- \frac{\partial}{\partial x_j} (\bar{C}_{ijrs} e_{rs}^x(\mathbf{v}_0)) = \langle f^{(0)} \rangle \quad (2.2.39)$$

where

$$\boxed{\bar{C}_{ijrs} = \langle C_{ijrs}^\varepsilon + C_{ijkl}^\varepsilon e_{kl}^y(\boldsymbol{\chi}^{rs}) \rangle} \quad (2.2.40)$$

The equation (2.2.39) is called the homogenized equation or macro level equilibrium equation and the equation (2.2.40) gives the homogenized coefficients or the effective elastic constants.

Knowing the solution of the cell problem ($\mathbf{u}^{(1)}$) and the effective stiffness, the effective

coefficient of thermal expansion, effective coefficient of shrinkage, and the state of micro-stresses are obtained as detailed in the following sections.

2.2.2 Effective coefficient of thermal expansion

The following formulation completely follows the work presented in [4], it is presented here for the sake of completeness. To find the effective coefficient of thermal expansion, consider the equation (2.2.25) with $\Delta T \neq 0$ and $\frac{\Delta V}{V} = 0$.

When $\mathbf{u}^{(0)}$ and $\mathbf{u}^{(1)}$ are known, the equation (2.2.25) with $\Delta T \neq 0$ and $\frac{\Delta V}{V} = 0$, can be written as

$$A_0 \mathbf{u}^{(2)} = f_i^{(0)} - A_1 \mathbf{u}^{(1)} - A_2 \mathbf{u}^{(0)} - \frac{\partial}{\partial x_j} (C_{ijkl}^\varepsilon \alpha_{kl}^\varepsilon \Delta T) \quad (2.2.41)$$

By virtue of the equations (2.2.26) and (2.2.27), y-periodic solution $\mathbf{u}^{(2)}$ exists if and only if

$$\left\langle f_i^{(0)} - A_1 \mathbf{u}^{(1)} - A_2 \mathbf{u}^{(0)} - \frac{\partial}{\partial x_j} (C_{ijkl}^\varepsilon \alpha_{kl}^\varepsilon \Delta T) \right\rangle = 0 \quad (2.2.42)$$

Substituting for $\mathbf{u}^{(0)}$ and $\mathbf{u}^{(1)}$ from (2.2.28) and (2.2.30), the condition (2.2.42) yields

$$\begin{aligned} \int_Y \left\{ f^{(0)} + \frac{\partial}{\partial x_j} ([C_{ijrs}^\varepsilon + C_{ijkl}^\varepsilon e_{kl}^y(\boldsymbol{\chi}^{rs})] e_{rs}^x(\mathbf{v}_0)) - \frac{\partial}{\partial x_j} (C_{ijkl}^\varepsilon \alpha_{kl}^\varepsilon \Delta T) + \right. \\ \left. + \frac{1}{2} \frac{\partial}{\partial y_j} (C_{ijkl}^\varepsilon \chi_k^{rs}) \frac{\partial}{\partial x_l} (e_{rs}^x(\mathbf{v}_0)) + \frac{1}{2} \frac{\partial}{\partial y_j} (C_{ijkl}^\varepsilon \chi_l^{rs}) \frac{\partial}{\partial x_k} (e_{rs}^x(\mathbf{v}_0)) + \right. \\ \left. + e_{kl}^x(\mathbf{w}_1) \frac{\partial}{\partial y_j} (C_{ijkl}^\varepsilon) \right\} dy = 0 \end{aligned} \quad (2.2.43)$$

The functions C_{ijkl} and $\boldsymbol{\chi}^{rs}$ are y-periodic and the functions $e_{kl}^x(\mathbf{w}_1)$, $\frac{\partial}{\partial x_i} (e_{rs}^x(\mathbf{v}_0))$ and $\frac{\partial}{\partial x_k} (e_{rs}^x(\mathbf{v}_0))$ are independent of \mathbf{y} . Therefore, by Gauss divergence theorem, the fourth, fifth and sixth terms of equation (2.2.43) vanish yielding the following.

$$\int_Y f^{(0)} dy + \frac{\partial}{\partial x_j} \left(\left\langle \int_Y [C_{ijrs}^\varepsilon + C_{ijkl}^\varepsilon e_{kl}^y(\boldsymbol{\chi}^{rs})] dy \right\rangle e_{rs}^x(\mathbf{v}_0) \right) - \frac{\partial}{\partial x_j} \int_Y C_{ijkl}^\varepsilon \alpha_{kl}^\varepsilon \Delta T dy = 0 \quad (2.2.44)$$

or

$$-\bar{C}_{ijrs} \frac{\partial}{\partial x_j} (e_{rs}^x(\mathbf{v}_0)) + \frac{\partial}{\partial x_j} b_{ij} \Delta T = \langle f^{(0)} \rangle \quad (2.2.45)$$

where

$$\bar{C}_{ijrs} = \langle C_{ijrs}^\varepsilon + C_{ijkl}^\varepsilon e_{kl}^y(\boldsymbol{\chi}^{rs}) \rangle \quad (2.2.46)$$

$$b_{ij} = \langle C_{ijkl}^\varepsilon \alpha_{kl}^\varepsilon \rangle = C_{ijkl}^f \alpha_{kl}^f v_f + C_{ijkl}^m \alpha_{kl}^m v_m \quad (2.2.47)$$

v_f = volume fraction of the fiber

v_m = volume fraction of the matrix

Consider the situation where there is only thermal load and the material has no external constraints. This results in non-zero strains and zero stresses at the macro level. But the micro stresses are non-zero due to the difference in the coefficient of thermal expansions of the constituent materials. With no external load, the equation (2.2.45) becomes,

$$-\frac{\partial}{\partial x_j} (\bar{C}_{ijrs} e_{rs}^x(\mathbf{v}_0)) + \frac{\partial}{\partial x_j} b_{ij} \Delta T = 0 \quad (2.2.48)$$

or

$$\frac{\partial}{\partial x_j} \bar{C}_{ijrs} (e_{rs}^x(\mathbf{v}_0) - \bar{\alpha}_{rs} \Delta T) = 0 \quad (2.2.49)$$

therefore, by equation (2.2.49)

$$e_{rs}^x(\mathbf{v}_0) = \bar{\alpha}_{rs} \Delta T \quad (2.2.50)$$

where

$$\bar{\alpha}_{rs} = [\bar{C}_{ijrs}]^{-1} b_{ij} \quad (2.2.51)$$

The equation (2.2.49) is called the homogenized equation or macro level equilibrium equation with only thermal loading and equation (2.2.51) gives the effective thermal coefficient of expansion. \bar{C}_{ijrs} is known from the solution of the cell problem.

By using similar arguments given in this section, the effective coefficient of shrinkage is obtained in the following section.

2.2.3 Effective shrinkage coefficient

To obtain the effective shrinkage coefficient, consider the equation (2.2.25) with $\Delta T = 0$ and $\frac{\Delta V}{V} \neq 0$.

When $\mathbf{u}^{(0)}$ and $\mathbf{u}^{(1)}$ are known, the equation (2.2.25) with $\Delta T = 0$ and $\frac{\Delta V}{V} \neq 0$, can be written as

$$A_0 \mathbf{u}^{(2)} = f_i^{(0)} - A_1 \mathbf{u}^{(1)} - A_2 \mathbf{u}^{(0)} - \frac{\partial}{\partial x_j} \left(C_{ijkl}^\varepsilon \eta_{kl}^\varepsilon \frac{\Delta V}{V} \right) \quad (2.2.52)$$

By virtue of the equations (2.2.26) and (2.2.27), y-periodic solution $\mathbf{u}^{(2)}$ exists if and only if

$$\left\langle f_i^{(0)} - A_1 \mathbf{u}^{(1)} - A_2 \mathbf{u}^{(0)} - \frac{\partial}{\partial x_j} \left(C_{ijkl}^\varepsilon \eta_{kl}^\varepsilon \frac{\Delta V}{V} \right) \right\rangle = 0 \quad (2.2.53)$$

Substituting for $\mathbf{u}^{(0)}$ and $\mathbf{u}^{(1)}$ from (2.2.28) and (2.2.30), the condition (2.2.53) yields

$$\begin{aligned} & \int_Y \left\{ f_i^{(0)} + \frac{\partial}{\partial x_j} \left([C_{ijrs}^\varepsilon + C_{ijkl}^\varepsilon e_{kl}^y(\boldsymbol{\chi}^{rs})] e_{rs}^x(\mathbf{v}_0) \right) - \frac{\partial}{\partial x_j} \left(C_{ijkl}^\varepsilon \eta_{kl}^\varepsilon \frac{\Delta V}{V} \right) + \right. \\ & \quad + \frac{1}{2} \frac{\partial}{\partial y_j} (C_{ijkl}^\varepsilon \boldsymbol{\chi}_k^{rs}) \frac{\partial}{\partial x_l} (e_{rs}^x(\mathbf{v}_0)) + \frac{1}{2} \frac{\partial}{\partial y_j} (C_{ijkl}^\varepsilon \boldsymbol{\chi}_l^{rs}) \frac{\partial}{\partial x_k} (e_{rs}^x(\mathbf{v}_0)) + \\ & \quad \left. + e_{kl}^x(\mathbf{w}_1) \frac{\partial}{\partial y_j} (C_{ijkl}^\varepsilon) \right\} dy = 0 \end{aligned} \quad (2.2.54)$$

The functions C_{ijkl} and $\boldsymbol{\chi}^{rs}$ are y-periodic and the functions $e_{kl}^x(\mathbf{w}_1)$, $\frac{\partial}{\partial x_l} (e_{rs}^x(\mathbf{v}_0))$ and $\frac{\partial}{\partial x_k} (e_{rs}^x(\mathbf{v}_0))$ are independent of y. Therefore, by Gauss divergence theorem, the fourth,

fifth and sixth terms of equation (2.2.54) vanish yielding the following.

$$\int_Y f^{(0)} dy + \frac{\partial}{\partial x_j} \left(\left\{ \int_Y [C_{ijrs}^\varepsilon + C_{ijkl}^\varepsilon e_{kl}^y(\boldsymbol{\chi}^{rs})] dy \right\} e_{rs}^x(\mathbf{v}_0) \right) - \frac{\partial}{\partial x_j} \int_Y C_{ijkl}^\varepsilon \eta_{kl}^\varepsilon \frac{\Delta V}{V} dy = 0 \quad (2.2.55)$$

or

$$-\frac{\partial}{\partial x_j} (\bar{C}_{ijrs} e_{rs}^x(\mathbf{v}_0)) + \frac{\partial}{\partial x_j} g_{ij} \Delta T = \langle f^{(0)} \rangle \quad (2.2.56)$$

where

$$\bar{C}_{ijrs} = \langle C_{ijrs}^\varepsilon + C_{ijkl}^\varepsilon e_{kl}^y(\boldsymbol{\chi}^{rs}) \rangle \quad (2.2.57)$$

$$g_{ij} = \langle C_{ijkl}^\varepsilon \eta_{kl}^\varepsilon \rangle = C_{ijkl}^f \eta_{kl}^f v_f + C_{ijkl}^m \eta_{kl}^m v_m \quad (2.2.58)$$

v_f = volume fraction of the fiber

v_m = volume fraction of the matrix

Let us consider the situation where there is only shrinkage load and the material has no external constraints. This results in non-zero strains and zero stresses at the macro level. But the micro stresses are non-zero due to the difference in the coefficient of shrinkage of the constituent materials. With no external load, the equation (2.2.56) becomes,

$$-\frac{\partial}{\partial x_j} (\bar{C}_{ijrs} e_{rs}^x(\mathbf{v}_0)) + \frac{\partial}{\partial x_j} g_{ij} \Delta T = 0 \quad (2.2.59)$$

or

$$\frac{\partial}{\partial x_j} \bar{C}_{ijrs} (e_{rs}^x(\mathbf{v}_0) - \bar{\eta}_{rs} \Delta T) = 0 \quad (2.2.60)$$

therefore, by equation (2.2.60)

$$e_{rs}^x(\mathbf{v}_0) = \bar{\eta}_{rs} \Delta T \quad (2.2.61)$$

where

$$\bar{\eta}_{rs} = [\bar{C}_{ijrs}]^{-1} g_{ij} \quad (2.2.62)$$

The equation (2.2.60) is called the homogenized equation or macro level equilibrium equation with only shrinkage loading and equation (2.2.62) gives the effective shrinkage coefficient. \bar{C}_{ijrs} is known from the solution of the cell problem.

Once the effective properties and the homogenized equation are obtained, the state of stress and strain at the macro level can be computed. Relation between the macro and the micro stress (and strain) is necessary to obtain the state of stress (and strain) at the micro level. This relation can be given in terms of concentration factors. The process of obtaining the strain concentration factors is described in the following section.

2.2.4 Strain concentration factors and state of stress (and strain) at micro level

Starting from the expression for strain at the micro level, the relation between macro and micro state of strain can be established. The expression for strain at the micro level, given by equation (2.2.14), is repeated here for reference.

$$e_{kl}(\mathbf{u}^\varepsilon) = e_{kl}^x(\mathbf{u}(\mathbf{x}, \mathbf{y})) + \frac{1}{\varepsilon} e_{kl}^y(\mathbf{u}(\mathbf{x}, \mathbf{y})) \quad (2.2.63)$$

Substituting the definitions (2.2.15), (2.2.16) and (2.2.21) in (2.2.63) and collecting different powers of ε separately yields,

$$e_{kl}(\mathbf{u}^\varepsilon) = \frac{1}{\varepsilon} e_{kl}^y(\mathbf{u}^{(0)}) + e_{kl}^x(\mathbf{u}^{(0)}) + e_{kl}^y(\mathbf{u}^{(1)}) + \varepsilon [e_{kl}^x(\mathbf{u}^{(1)}) + e_{kl}^y(\mathbf{u}^{(2)})] \quad (2.2.64)$$

By using (2.2.28), the first term in equation (2.2.64) becomes zero.

$$e_{kl}^y(\mathbf{u}^{(0)}) = 0 \quad (2.2.65)$$

Therefore, the lowest order approximation of strain at the micro level is given by,

$$e_{kl}(\mathbf{u}^\varepsilon) = e_{kl}^x(\mathbf{u}^{(0)}) + e_{kl}^y(\mathbf{u}^{(1)}) \quad (2.2.66)$$

By using (2.2.30), the above equation yields,

$$e_{kl}(\mathbf{u}^\varepsilon) = e_{kl}^x(\mathbf{u}^{(0)}) + e_{kl}^y(-\boldsymbol{\chi}^{rs}(\mathbf{y})e_{rs}^x(\mathbf{u}^{(0)})) \quad (2.2.67)$$

$$\Rightarrow \boxed{e_{kl}(\mathbf{u}^\varepsilon) = M_{klrs}e_{rs}^x(\mathbf{u}^{(0)})} \quad (2.2.68)$$

where

$$\boxed{M_{klrs} = [\delta_{rk}\delta_{sl} - e_{kl}^y(\boldsymbol{\chi}^{rs}(\mathbf{y}))]} \quad (2.2.69)$$

The relation between the macro strain and the micro strain through the strain concentration factor matrix M_{klrs} is given by (2.2.68). The micro strains and stresses, due to thermal, chemical shrinkage or mechanical loading can be obtained using this equation. The formulation developed in this chapter was implemented in a code by [4], using finite element method, to obtain the effective properties and the local fields for a damaged and undamaged continuum.

Chapter 3

Models for Macro Influence of Damage

3.1 Micromechanics on unit-cell RVE

The homogenization method is used to perform a micromechanical analysis on unit-cell RVE. This analysis is aimed at understanding the influence of volume fraction and damage on the effective elastic properties. The influences are studied by comparing the results of the analysis against the results obtained for a reference configuration. In the present study, the undamaged material having fiber volume fraction 0.608 is chosen as the reference configuration.

The parametric studies conducted to study the influences are:

1. Effect of volume fraction on the elastic properties of the undamaged composites.
2. Effect of damage modes and variation of damage sizes on the effective properties of the composites, at the reference volume fraction and also at other volume fractions.

Through this study a damage based model for property reduction is sought, the

effective elastic properties are defined as a smooth function of volume fraction and damage as:

$$E = E(v_f, d_i), \quad (3.1.1)$$

$$i = 1, 2, \dots, \text{total number of damage modes},$$

from which the change in effective elastic properties is obtained using a Taylor series expansion about the reference configuration in terms of the change in volume fraction from the reference volume fraction, Δv_f , and the increase in damage size from the undamaged configuration, Δd_i .

The Taylor series expansion of the equation (3.1.1) about the reference volume fraction is given by,

$$\begin{aligned} E(0.608 + v_f, 0.0 + d_i) \approx & E(0.608, 0.0) + \frac{\partial E}{\partial v_f} \Delta v_f + \sum_{i=1}^3 \left\{ \frac{\partial E}{\partial d_i} \Delta d_i \right\} + \\ & \frac{1}{2!} \frac{\partial^2 E}{\partial v_f^2} \Delta v_f^2 + \frac{1}{2!} \sum_{i=1}^3 \left\{ \frac{\partial^2 E}{\partial d_i^2} \Delta d_i^2 \right\} + \frac{1}{2!} \sum_{i=1}^3 \left\{ 2 \frac{\partial^2 E}{\partial v_f \partial d_i} \Delta v_f \Delta d_i \right\} \end{aligned} \quad (3.1.2)$$

this can be re-written in terms of Δd_i and Δv_f as follows

$$\Delta E = [j_1 \Delta v_f + j_2 \Delta v_f^2] + \sum_{i=1}^3 [k_{1i} \Delta d_i + k_{2i} \Delta d_i^2] + \sum_{i=1}^3 [p_i \Delta v_f \Delta d_i] \quad (3.1.3)$$

Then the damaged effective elastic properties are given in terms of undamaged elastic properties, E^{ud} , as

$$E^d = E^{ud} + \Delta E \quad (3.1.4)$$

where, $\Delta E = E(0.608 + \Delta v_f, 0.0 + \Delta d_i) - E(0.608, 0.0)$, j_1 , j_2 , k_{1i} , k_{2i} and p_i are the coefficients of Δv_f , Δv_f^2 , Δd_i , Δd_i^2 and $\Delta v_f \Delta d_i$ respectively, in equation (3.1.4)

The values of j_1 , j_2 , k_{1i} , k_{2i} and p_i are determined from the numerical experiments as described below.

Determination of j_1 and j_2 :

Consider the condition when $d_i = 0$, $i = 1,2,3,4$. The expression in (3.1.3) reduces to:

$$\Delta E \approx j_1 \Delta v_f + j_2 \Delta v_f^2 \quad (3.1.5)$$

The constants j_1 and j_2 are obtained using a quadratic least square fit.

Determination of k_{1i} and k_{2i} :

Consider the condition when $v_f = 0$, $i = 1,2,3,4$. The expression in (3.1.3) reduces to:

$$\Delta E \approx k_{1i} \Delta d_i + k_{2i} \Delta d_i^2 \quad (3.1.6)$$

Hence, numerical computations over damaged RVE, at the reference volume fraction, are required to obtain the coefficients, k_{1i} and k_{2i} . By considering one damage mode at a time, the constants k_{1i} and k_{2i} , corresponding to mode 'i', can be obtained from a quadratic fit of the plot between the change in elastic constants and the change in damage size for the damage mode 'i'.

Determination of p_i :

Knowing the values of j_1 , j_2 , k_{1i} , and k_{2i} , the coupling coefficient p_i for the damage type 'i' can be obtained as follows. Equation (3.1.3) can be rewritten to get,

$$\Delta E - [j_1 \Delta v_f + j_2 \Delta v_f^2] + [k_{1i} \Delta d_i + k_{2i} \Delta d_i^2] = p_i \Delta v_f \Delta d_i \quad (3.1.7)$$

Now by considering one damage mode 'i' at a time, the constant p_i can be obtained from a linear fit between the left hand side and the right hand side of the above equation over all possible combinations of Δv_f and Δd_i considered for the analysis. Provided all the constants are determined, equation (3.1.3) gives the change in elastic constants for a given change in volume fraction and a given change in the damage size of a given damage mode. Once the change in elastic constants are obtained, the damaged elastic constants can be obtained from equation (3.1.1).

To verify the capability of the models, the damaged elastic properties are computed using the detailed model for different damages and damage sizes, at reference and other volume fractions. The computed values are then compared with the values that are obtained from homogenization. The plots showing comparison of elastic properties, computed using the detailed and homogenization, with the results of the numerical experiments are given in figures (3.2 to 3.2).

The two independent, orthogonal matrix cracks studied are shown in figure 3.1

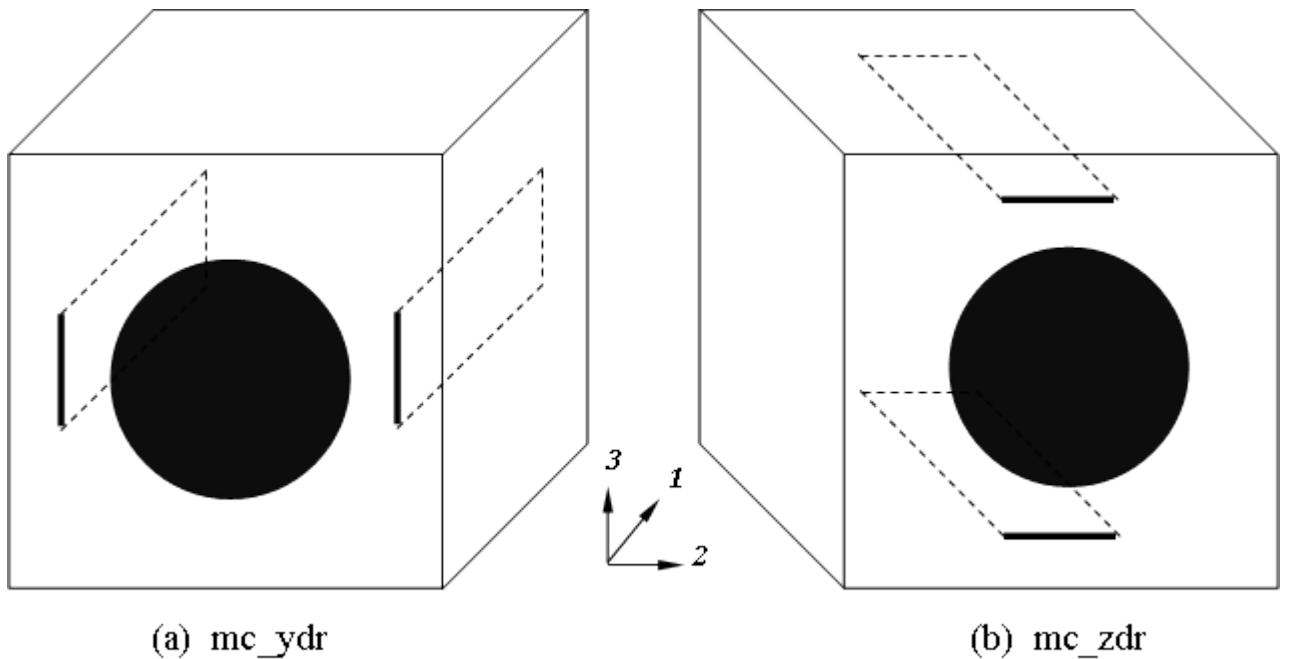


Figure 3.1: a.) Matrix crack mc-ydr and b.) Matrix crack mc-zdr

3.2 Effects of transverse matrix cracks under study on the effective properties at reference volume fraction($v_f=0.608$)

To study the effect of matrix cracks (figure 3.1) on the effective properties, a series of numerical experiments are conducted on the unit-cell RVE with different sizes, one at a

time, at the reference volume fraction. As the study is conducted at the reference volume fraction, the change in volume fraction is zero ($\Delta v_f = 0$). Now, equation 3.1.3 reduces to

$$\Delta E \approx k_{1i}\Delta d_i + k_{2i}\Delta d_i^2 \quad (3.2.1)$$

The values of the coefficients in the above equation can be obtained using various combinations of damage sizes at reference volume fraction and the corresponding stiffness constants. The materials considered for the analysis are glass/epoxy and carbon/epoxy composites. The different types of damages considered are: a) fiber breakage [4]; b) fiber matrix de-bond [4]; and c) matrix cracks (figure 3.1).

The values for j_1 , j_2 , k_{1i} and k_{2i} for matrix cracks in y and z directions considered in this study are listed in tables 3.1 to 3.3.

The effect of matrix cracks (figure 3.1) on effective properties, at reference volume fraction, are consolidated in figures 3.2 to 3.2 for glass/epoxy and carbon/epoxy composites respectively. From the plots shown it can be inferred that:

1. E_{22} is primarily affected and G_{12} is also affected by the matrix crack (mc-ydr) in y-direction.
2. E_{33} is primarily affected and G_{13} is also affected by the matrix crack (mc-zdr) in z-direction.
3. With change in volume fractions similar trends are observed for both the matrix cracks.
4. With change in the material (glass/epoxy) similar observations are noted.

Table 3.1: Least square quadratic fit data values (j_1 and j_2) corresponding to carbon/epoxy and glass/epoxy composites.

<i>Material</i>		k_1	k_2
carbon/epoxy	E_{11}	226.968	7.1801
	E_{22}	36.4889	40.9412
	E_{33}	36.4889	40.9412
	G_{23}	8.434	13.461
	G_{13}	16.1612	25.9022
	G_{12}	16.1612	25.9022
	ν_{23}	-0.2524	0.3102
	ν_{13}	-0.1042	-0.0056
	ν_{12}	-0.1042	-0.0056
	glass/epoxy	E_{11}	82.7994
E_{22}		65.715	102.2174
E_{33}		65.71	102.217
G_{23}		11.9218	21.7945
G_{13}		19.2934	33.2271
G_{12}		19.2934	33.2271
ν_{23}		-0.5686	-0.0993
ν_{13}		-0.1399	-0.0196
ν_{12}		-0.1399	-0.0196

3.3 Free energy density function

The free energy density function for a damaged composite in terms of the damaged elastic properties on the lines of [4] can be written as follows:

$$\begin{aligned}
\psi^d = & \frac{1}{2} \left\{ \frac{\sigma_{11}^2}{E_{11}^d} + \frac{\sigma_{22}^2}{E_{22}^d} + \frac{\sigma_{33}^2}{E_{33}^d} - \left(\frac{\nu_{21}^d}{E_{22}^d} + \frac{\nu_{12}^d}{E_{11}^d} \right) \sigma_{11} \sigma_{22} \right\} \\
& - \frac{1}{2} \left\{ \left(\frac{\nu_{31}^d}{E_{33}^d} + \frac{\nu_{13}^d}{E_{11}^d} \right) \sigma_{11} \sigma_{33} - \left(\frac{\nu_{32}^d}{E_{33}^d} + \frac{\nu_{23}^d}{E_{22}^d} \right) \sigma_{22} \sigma_{33} \right\} \\
& + \frac{1}{2} \left\{ \frac{2\sigma_{12}^2}{G_{12}^d} + \frac{2\sigma_{13}^2}{G_{13}^d} + \frac{2\sigma_{23}^2}{G_{23}^d} \right\}
\end{aligned} \tag{3.3.1}$$

where, the superscript 'd' denotes the values that correspond to the damaged configuration. The macrolevel effective properties behave according to the model given by the

Table 3.2: Least square quadratic fit data values (k_1 , k_2 and p) corresponding to matrix crack ($mc - ydr$) for carbon/epoxy and glass/epoxy composites.

<i>Material</i>		k_1	k_2	p
carbon/epoxy	E_{11}	-0.7424	0.6725	0.1076
	E_{22}	-19.8951	5.3988	-34.4426
	E_{33}	-1.1931	0.4593	-0.6132
	G_{23}	-1.1205	-1.7002	-5.9568
	G_{13}	-0.0043	-0.0161	-0.0377
	G_{12}	-6.8028	1.8324	-15.2187
	ν_{23}	-0.1703	-0.1266	0.0157
	ν_{13}	-0.0067	0.0038	-0.0044
	ν_{12}	0.0331	-0.011	0.0519
glass/epoxy	E_{11}	-0.285	0.2545	0.0047
	E_{22}	-31.7601	13.3375	-61.2823
	E_{33}	-2.2464	0.9361	-2.5397
	G_{23}	-1.6198	-1.7216	-8.2859
	G_{13}	-0.0054	-0.0187	-0.051
	G_{12}	-7.9776	2.595	-18.0078
	ν_{23}	-0.0462	-0.1613	0.2515
	ν_{13}	-0.0104	0.0062	-0.0075
	ν_{12}	0.048	-0.0178	0.0785

equations [4] which can be written as:

$$E_{ij}^d = E_{ij}^d(d_1, d_2, d_3), \text{ when } \sigma_{11}, \sigma_{22} \text{ or } \sigma_{33} > 0 \quad (3.3.2)$$

$$E_{ij}^d = E_{ij}^d(0, d_2, d_3), \text{ when } \sigma_{11} < 0, \sigma_{22} \text{ or } \sigma_{33} > 0 \quad (3.3.3)$$

$$E_{ij}^d = E_{ij}^d(d_1, d_2, 0), \text{ when } \sigma_{11} > 0, \sigma_{22} \text{ or } \sigma_{33} < 0 \quad (3.3.4)$$

$$E_{ij}^d = E_{ij}^d(0, d_2, 0), \text{ when } \sigma_{11}, \sigma_{22} \text{ and } \sigma_{33} < 0 \quad (3.3.5)$$

When the normal stress σ_{11} is compressive, there is complete load transfer across a broken fiber and hence the loss of stiffness will not be seen at the macrolevel. Similarly, when σ_{22} and σ_{33} are compressive, the loss of stiffness due to d_3 will not be observed at the macrolevel. The free energy density as reported in [4] decreases with the increase in

Table 3.3: Least square quadratic fit data values (k_1 , k_2 and p) corresponding to matrix crack ($mc - zdr$) for carbon/epoxy and glass/epoxy composites.

<i>Material</i>		k_1	k_2	p
carbon/epoxy	E_{11}	-0.7425	0.6725	0.1072
	E_{22}	-1.2133	0.4728	-0.7155
	E_{33}	-19.9202	5.4253	-34.581
	G_{23}	-1.1254	-1.6949	-5.9843
	G_{13}	-6.7897	1.8204	-15.2277
	G_{12}	-0.0003	-0.0183	-0.028
	ν_{23}	0.3085	0.0632	0.072
	ν_{13}	0.0331	-0.011	0.0528
	ν_{12}	-0.0066	0.0038	-0.0045
glass/epoxy	E_{11}	-0.2852	0.2546	0.0042
	E_{22}	-2.2886	0.9664	-2.7169
	E_{33}	-31.8011	13.3835	-61.4501
	G_{23}	-1.6259	-1.7146	-8.3153
	G_{13}	-7.9634	2.5818	-18.0171
	G_{12}	-0.0005	-0.0213	-0.0382
	ν_{23}	0.4463	0.0537	0.3324
	ν_{13}	0.0481	-0.0177	0.0796
	ν_{12}	-0.0103	0.0062	-0.0076

damage for all damage modes and in all cases of loading. That is, $-\frac{d\psi}{d(d_i)} > 0$. This result was used while deriving the evolution law for different damage modes.

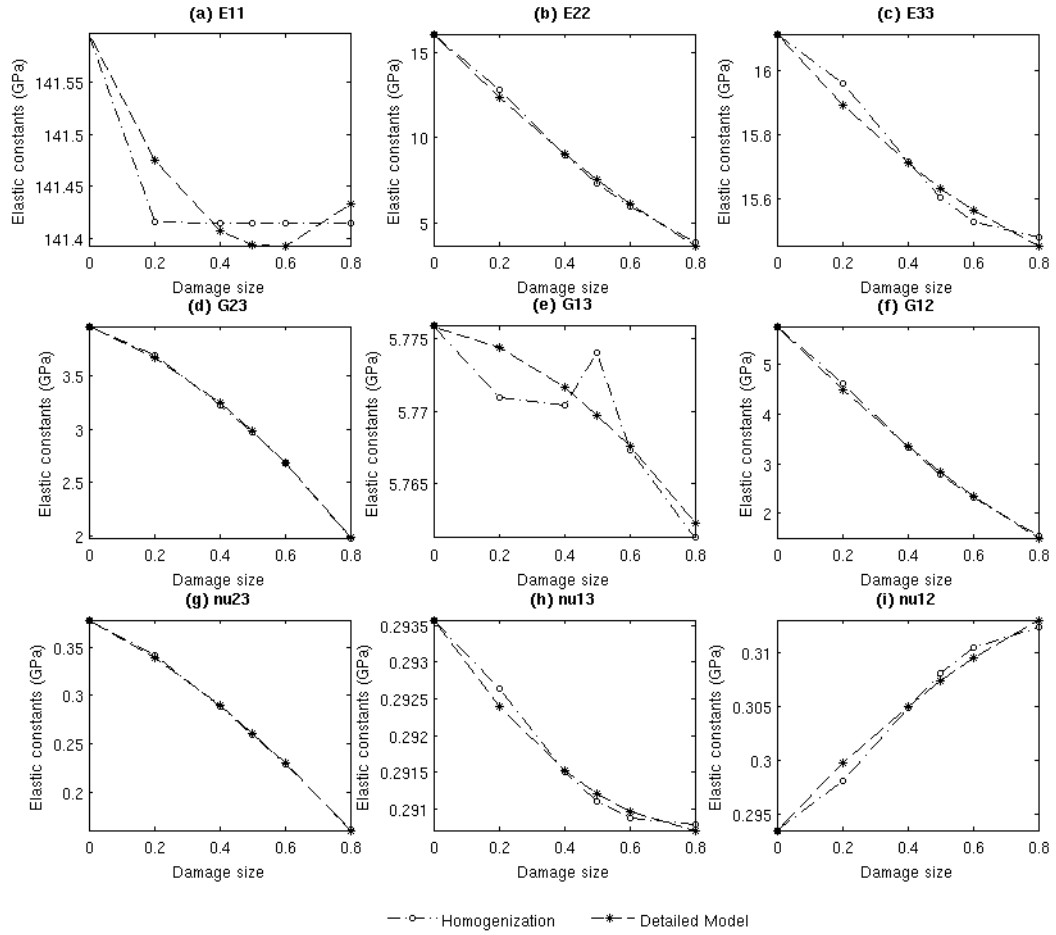


Figure 3.2: Elastic properties of *carbon/epoxy* composite with $mc - ydr$; $\Delta v_f = 0$: Comparison of homogenization and detailed models

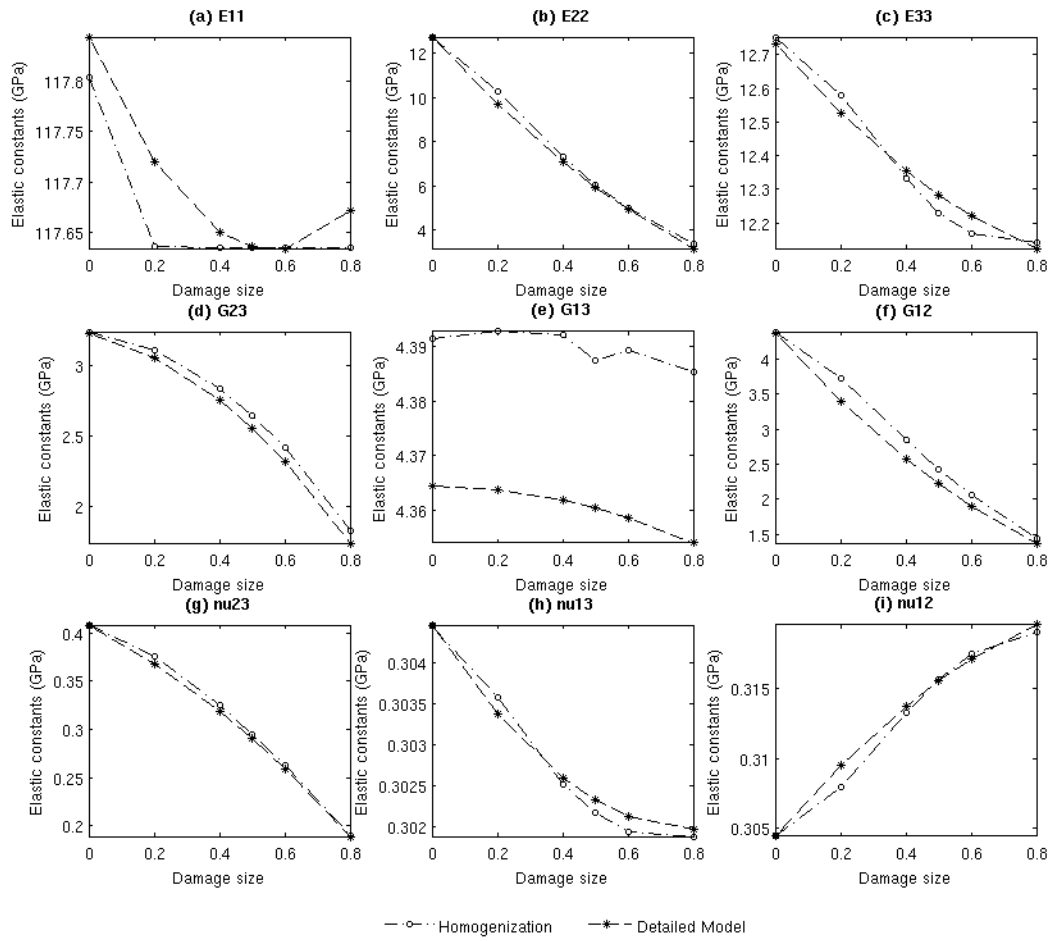


Figure 3.3: Elastic properties of *carbon/epoxy* composite with $mc - ydr$; $\Delta v_f = -105$: Comparison of homogenization and detailed models

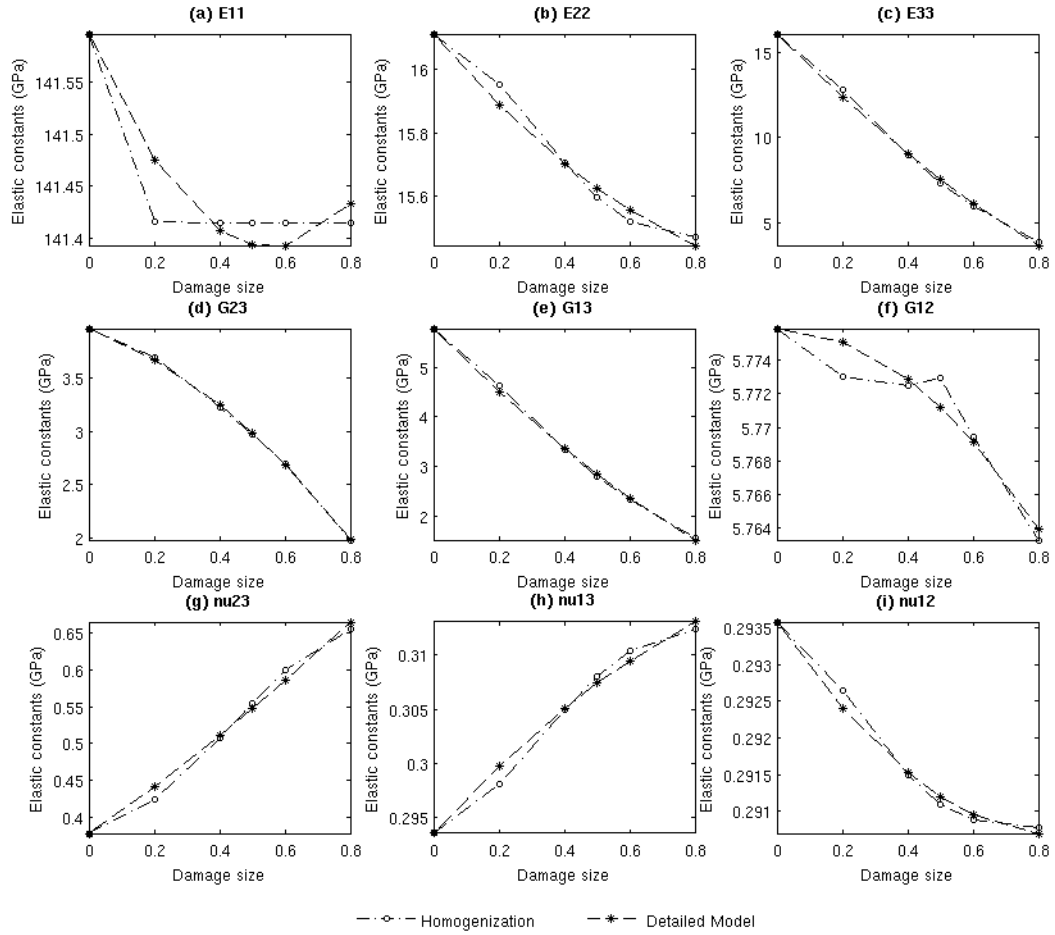


Figure 3.4: Elastic properties of *carbon/epoxy* composite with $mc - zdr$; $\Delta v_f = 0$: Comparison of homogenization and detailed models

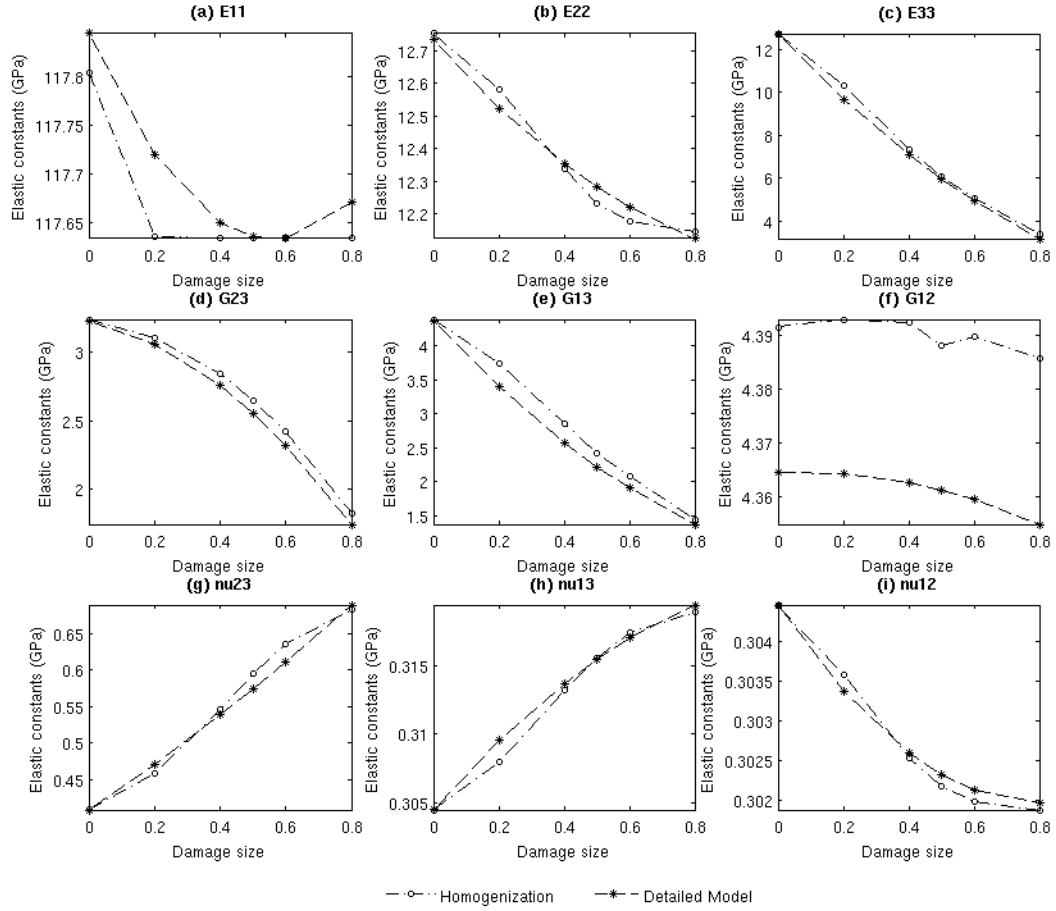


Figure 3.5: Elastic properties of *carbon/epoxy* composite with $mc - zdr$; $\Delta v_f = -105$: Comparison of homogenization and detailed models

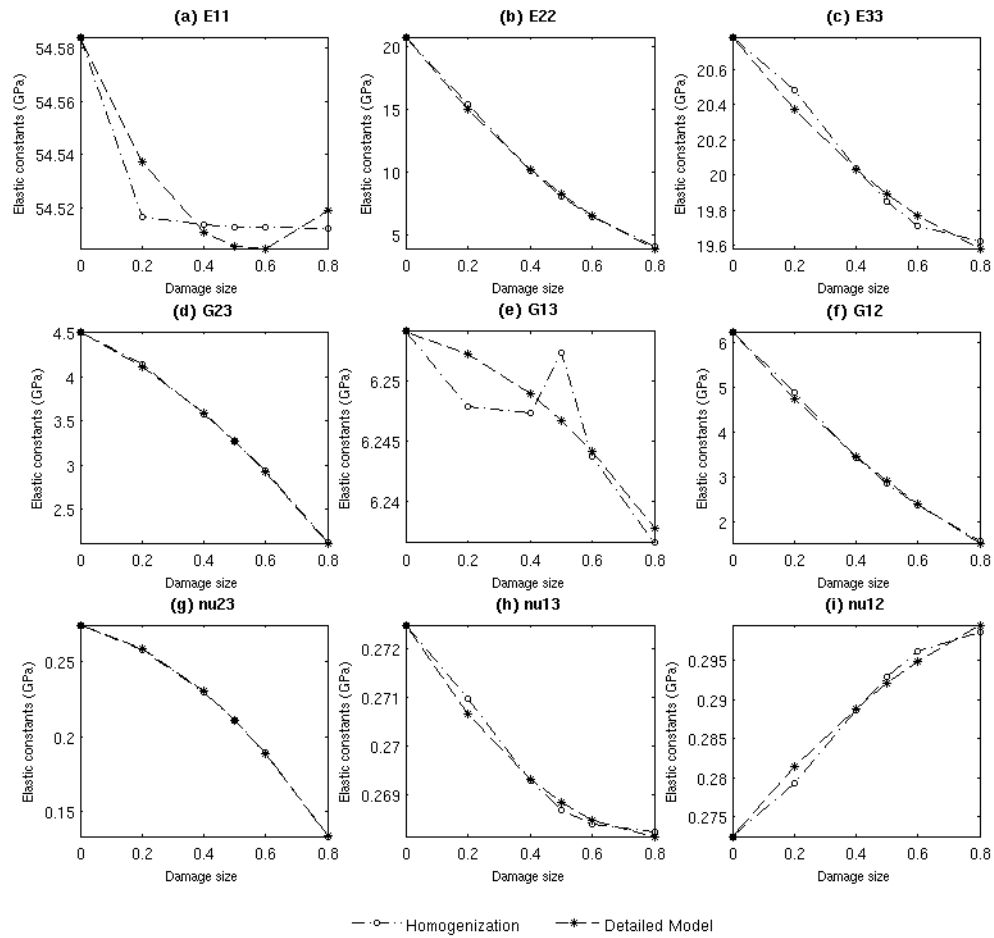


Figure 3.6: Elastic properties of *glass/epoxy* composite with $mc - ydr$; $\Delta v_f = 0$: Comparison of homogenization and detailed models

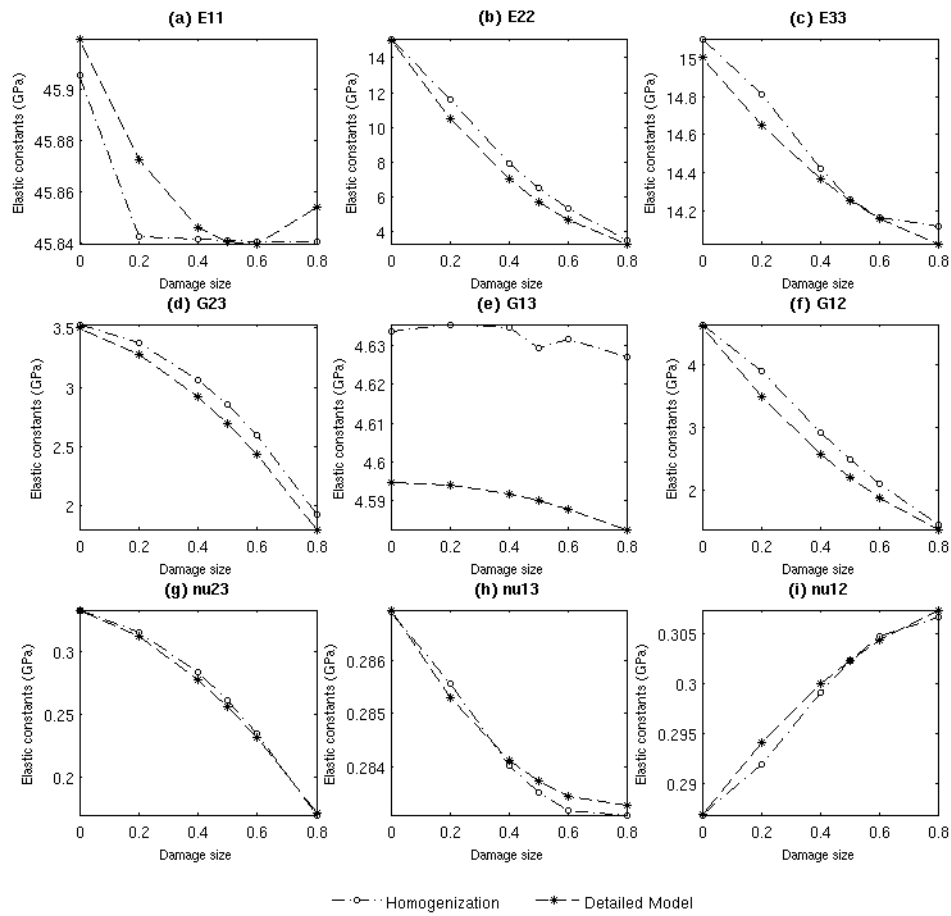


Figure 3.7: Elastic properties of *glass/epoxy* composite with $mc - ydr$; $\Delta v_f = -105$: Comparison of homogenization and detailed models

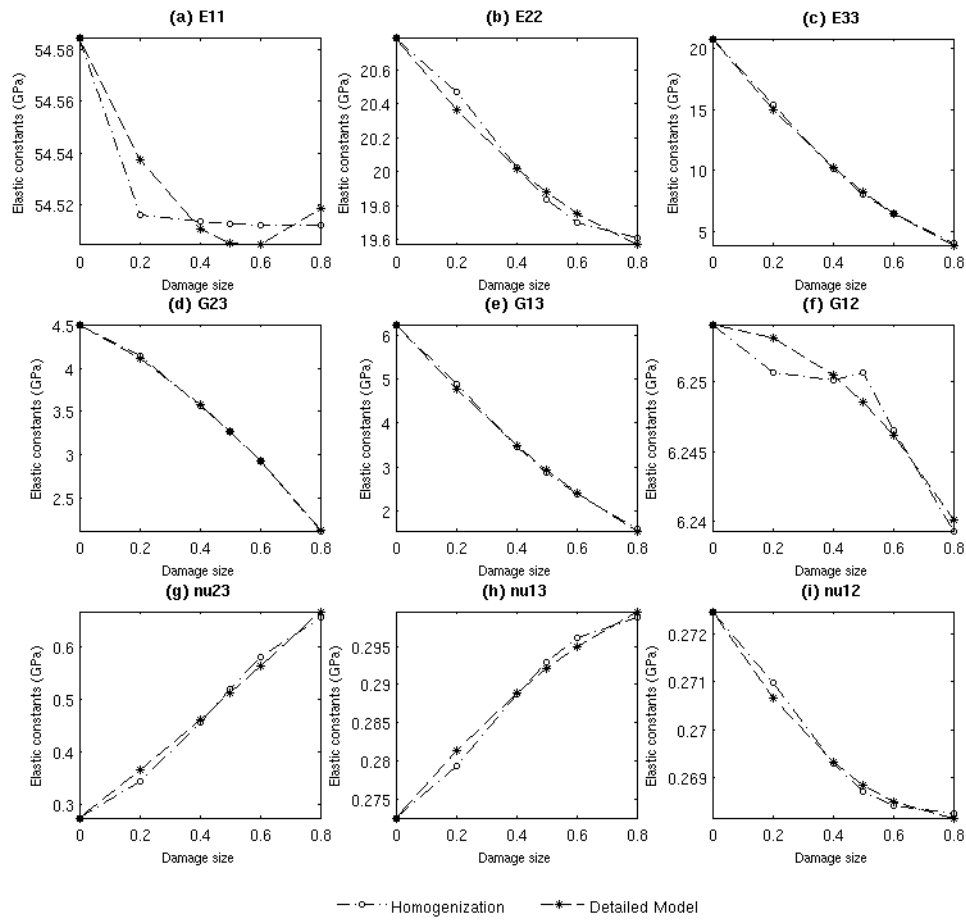


Figure 3.8: Elastic properties of *glass/epoxy* composite with $mc - zdr$; $\Delta v_f = 0$: Comparison of homogenization and detailed models

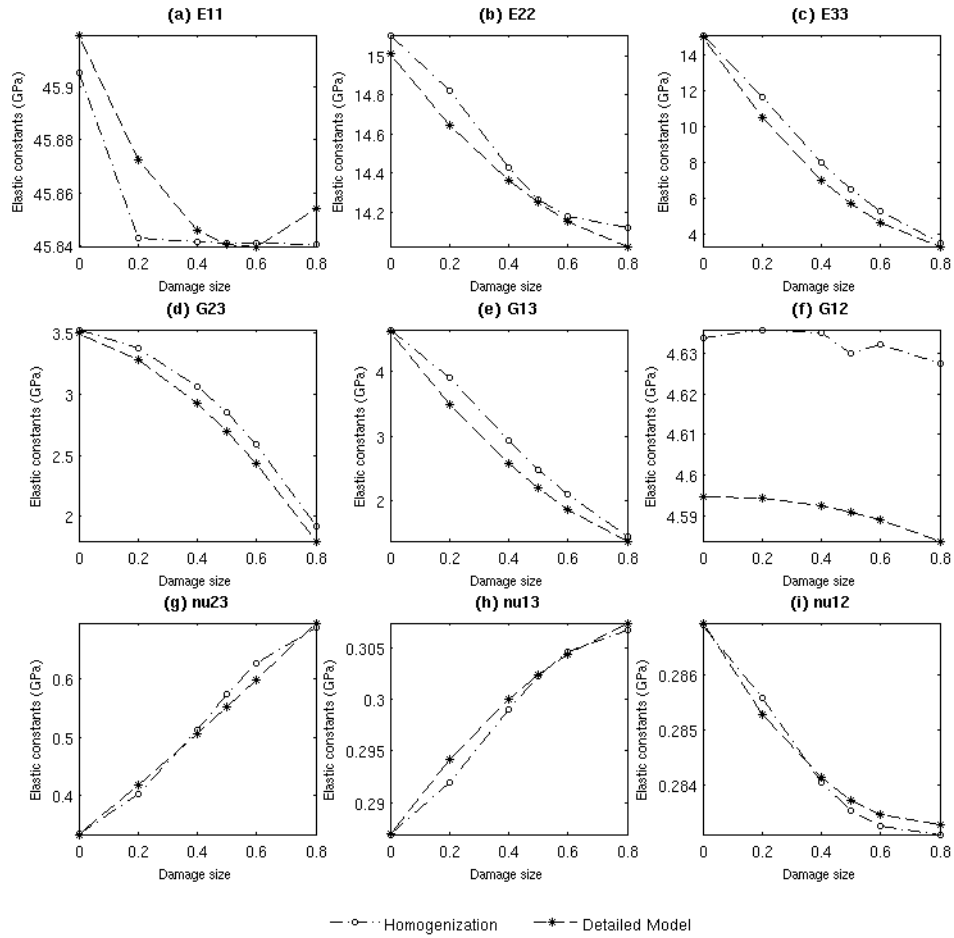


Figure 3.9: Elastic properties of *glass/epoxy* composite with $mc - zdr$; $\Delta v_f = -105$: Comparison of homogenization and detailed models

Chapter 4

Model Identification and Predictions

4.1 Model Identification

The model parameters were identified [4] using the same material, carbon/epoxy (T300/914) with $v_f = 0.6$, used by Ladeveze et al. [17]. The yield strength for matrix (σ_y^c) as used in the present study is 58.7 MPa and the stress at the fiber failure is 1000 Mpa, the initiation parameters were obtained from the same model. The initiation and growth of crack (mc-zdr) due to σ_{33} is not considered here, as it is assumed that the transverse stress components in the ply are negligible. The values of the initiation parameters are listed in table 4.1. The evolution model for d_1 is already known (see equation (1.2.4)).

Table 4.1: Initiation parameters of the model

$\sigma_{11}^{c,macro}(GPa)$	$\sigma_{22}^{c,macro}(GPa)$	$\sigma_{12}^{c,macro}(GPa)$	Λ
2.0000	0.0346	0.0205	0.8000

The damage parameters in the evolution models for d_2 and d_3 were determined from the mechanical response of the angle-ply laminates used in DML. The idea behind the selection of sequence of laminate configurations in DML is that with one configuration,

chosen appropriately such that only one of the damage mode is dominant, the evolution model for the corresponding damage mode can be obtained directly from the mechanical response. Knowing the evolution for one damage mode, the coupling parameter between the two damage modes and the evolution of other mode can be obtained by choosing a configuration where the two damage modes co-exists. In this study, the same configurations used in DML are employed, but the parameters are determined from the point of view of the model under study.

4.1.1 Determination of c_1

The evolution parameter c_1 is directly obtained from the ply failure model [4]. For the sake of completeness the process of obtaining the same is detailed here.

The same laminate configurations in [17] are used to determine the required parameters in the proposed model. For a highly orthotropic material such as T300/914 carbon/epoxy composite with $[\pm 45]_s$ laminate configuration, the relation between the lamina stresses in the material coordinates to the applied axial stress in the laminate is given by the following.

$$\sigma_{11} = 0.8753\bar{\sigma}_x; \quad \sigma_{22} = 0.1247\bar{\sigma}_x; \quad \sigma_{12} = -0.5\bar{\sigma}_x; \quad (4.1.1)$$

As failure due to σ_{11} occurs at a much higher value of $\bar{\sigma}$, it is obvious that the damage mode in the material is highly influenced by σ_{12} . So, the only dominant damage mode is d_2 . Thus, from the shear response of the composite lamina, the parameter in the evolution model for the damage mode d_2 is obtained by measuring shear modulus at different stress levels from the slope of the unloading/reloading curves corresponding to each stress level. The change in modulus, as compared to the initial modulus, at different stress levels is then calculated. The damage size of d_2 , that would result in the corresponding change in modulus, is obtained by using the proposed equation for finding elastic properties, with only $d_2 \neq 0$, at each stress level considered.

Knowing the values of d_2 , at different stress levels of σ_{12} , the parameter c_1 in the evolution

model is obtained from the best least square fit of the plot between d_2 and $\sigma_{12} - \sigma_{12}^c$. Here, σ_{12}^c is the stress at which the shear damage initiates.

4.1.2 Determination of c_2

The value of c_2 is determined by adopting the procedure as detailed in the model [4] under study. Laminate with $[\pm 67.5]_s$ configuration is chosen for the determination of c_2 . This laminate is found to have sufficiently low inter-laminar stresses, such that they do not cause initiation of delamination [1]. The relation between the lamina stresses in the material coordinates to the axial stress in the $[\pm 67.5]_s$ laminate is given by the following:

$$\sigma_{11} = 0.1148\bar{\sigma}_x; \quad \sigma_{22} = 0.8852\bar{\sigma}_x; \quad \sigma_{12} = -0.3219\bar{\sigma}_x; \quad (4.1.2)$$

Note that the state of stress is biaxial and therefore the two damage modes, d_2 and d_3 co-exist.

The experimental plot between σ_{22} and e_{22} , is used to determine c_2 . From the curve, the reduction in the modulus (E_{22}) at different levels of stress (σ_{22}) is obtained. The reduction in the modulus, ΔE_{22} , depends on both the damage modes d_2 and d_3 .

$$\Delta E_{22} \approx \left. \frac{\partial E_{22}}{\partial d_2} \right|_{v_f=0.6} \Delta d_2 + \left. \frac{\partial E_{22}}{\partial d_3} \right|_{v_f=0.6} \Delta d_3 \quad (4.1.3)$$

Using the evolution model for d_2 and σ_{12} that exist corresponding to the given value of σ_{22} , the reduction in E_{22} only due to d_2 , is obtained for different levels of σ_{22} . This reduction, $\left. \frac{\partial E_{22}}{\partial d_2} \right|_{v_f=0.6} \Delta d_2$, is deducted from the reduction, ΔE_{22} , measured directly from the experimental curve as follows.

$$\Delta E_{22}|_{d_3} \approx \Delta E_{22} - \left. \frac{\partial E_{22}}{\partial d_2} \right|_{v_f=0.6} \Delta d_2 \quad (4.1.4)$$

The resulting amount of reduction, $\Delta E_{22}|_{d_3}$, is used for the calculation of the damage size

d_3 in a way similar to the determination of d_2 . That is, the size of damage d_3 , that would result in the corresponding change in modulus (after deducting the reduction due to d_2), is obtained by using the proposed equation for finding elastic properties at each stress level considered.

Knowing the values of d_3 , at different stress levels of σ_{22} , the parameter c_2 in the evolution model is obtained from the least square fit for the plot between d_3 and $\sigma_{22} - \sigma_{22}^c$. σ_{22}^c is the stress at which the damage initiates. The values of evolution parameters are listed in table 4.2.

Table 4.2: Evolution parameters of the model

c_1	c_2
11.0	19.56

4.2 Model Predictions

The model [4] under study is used to predict the responses of several laminates, made of T300/914 carbon/ epoxy, such as: a) $[\pm 45]_s$, b) $[\pm 67.5]_s$, c) $[0/90]_s$ and d) $[-12/78]_{2s}$. The samples are loaded by either a monotonic or a cyclic stress profile, as given in figures 4.6, 4.12, 4.16 and 4.22. The experimental data in figures 4.2 to 4.24 are taken from [17].

1. $[\pm 45]_s$:

The prediction of tensile response of $[\pm 45]_s$ laminate and the shear response of a lamina are given in figures 4.2 and 4.4 respectively. The state of stress in the lamina given by equation (4.1.1) shows that the response of the lamina is influenced by the shear stress. Thus, the damage mode is likely to be the fiber-matrix de-bond. The growth of different damage modes is given in figure 4.5b, which shows that the only damage mode which is active is the fiber-matrix debond and the curves obtained are well in accord with the results of matrix crack [4]. The responses given in figures 4.1b and 4.3b match closely with the

results obtained by [4].

2. $[\pm 67.5]_s$:

The prediction of the shear and the transverse responses of a lamina, in $[\pm 67.5]_s$ laminate, are given in figures 4.8 and 4.10 respectively. Further, the state of stress in the lamina given by equation (4.1.2) shows a biaxial state of stress. Thus, a coupled state of damage (modes d_2 and d_3) is likely to be present. The growth of different damage modes given in figure 4.12 shows the presence of two damage modes, the fiber-matrix de-bond and the matrix cracks. The shear response matches well with the one obtained by the model [4], while the transverse response is stiffer than the experiment. This is expected and is due to the difference in the transverse properties used in the prediction and the experiment (refer 4.1).

The damage (d_3) due to the matrix crack (mc-ydr) has evolved to a lesser value as compared to the matrix crack considered in [4], this is observed because for a particular size of damage the area that can be damaged to the maximum extent is bigger in the present case as compared to the one considered in [4]. Fiber/matrix debond (d_2) has not changed compared to [4]. Damage mode corresponding to fiber-breakage is not triggered by this loading because of the high value of initiation stress, damage due to matrix crack (mc-zdr) stays unaffected because of the absence of σ_{33} loading.

Table 4.3: Differences in the lamina properties used in the model from the experiment

Lamina Properties		
	Model	Experiment
$E_{11}(GPa)$	141.5966	170.0000
$E_{22}(GPa)$	16.1131	10.8000
$G_{12}(GPa)$	5.7759	5.8000
$\nu_{12}(GPa)$	0.2936	0.3400

3. $[0/90]_s$:

The prediction of the tensile response of the $[0/90]_s$ laminate is given in figure 4.14.

The results are as expected, i.e., the 90° lamina fails first followed by the failure of 90° lamina. This can be seen from the growth of different damage modes given in figures 4.16 and 4.18, for 0° and 90° laminae respectively. The matrix cracks are first initiated in 90° lamina. The evolution of d_3 very quickly reaches the critical value of one in [4]. In the 0° lamina, matrix cracks initiate before the fiber breaks, the model [4] predicts similar such behaviour with the present transverse matrix cracks. Development of d_2 is not noticed in both laminae and the fiber breakage is noticed only in 0° lamina.

4. $[-12/78]_{2s}$:

Prediction of the tensile response of the $[-12/78]_{2s}$ laminate is given in figure 4.20. The state of stress in -12° and 78° laminae are given by (4.2.1) and (4.2.2) respectively, as:

$$\sigma_{11} = 1.7187\bar{\sigma}_x; \quad \sigma_{22} = 0.0545\bar{\sigma}_x; \quad \sigma_{12} = 0.2034\bar{\sigma}_x; \quad (4.2.1)$$

$$\sigma_{11} = 0.0319\bar{\sigma}_x; \quad \sigma_{22} = 0.1948\bar{\sigma}_x; \quad \sigma_{12} = -0.2034\bar{\sigma}_x; \quad (4.2.2)$$

σ_{22} has lesser influence on damage in -12° lamina, compared to σ_{12} , which can be seen from the plots showing the growth of damage (refer figure 4.22), where only the damage mode d_2 is present. In the case of 78° lamina, two damage modes, d_2 and d_3 are present (refer figure(4.24)). Further, the growth of damage mode d_3 saturates, as the values of transverse stress in the lamina saturates. The growth of damage mode d_2 is same in both the laminae and similar trend is observed as compared to [4]. The damage mode d_3 shows a similar movement as in [4] but, the saturation value drops below that of [4], this is as expected because of the definition of damage variable defined in both cases.

5. $[67.5/22.5]_{2s}$:

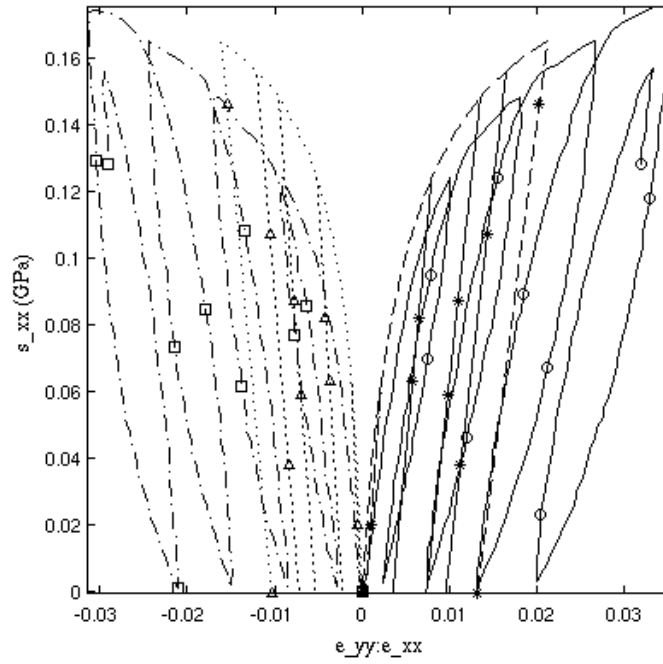
The prediction of the tensile response of the $[67.5/22.5]_{2s}$ is given in figure 4.26. The state of stress in 67.5° and 22.5° laminae are given by (4.2.3) and (4.2.4), respectively, as:

$$\sigma_{11} = -0.5195\bar{\sigma}_x; \quad \sigma_{22} = 0.4825\bar{\sigma}_x; \quad \sigma_{12} = 0.0171\bar{\sigma}_x; \quad (4.2.3)$$

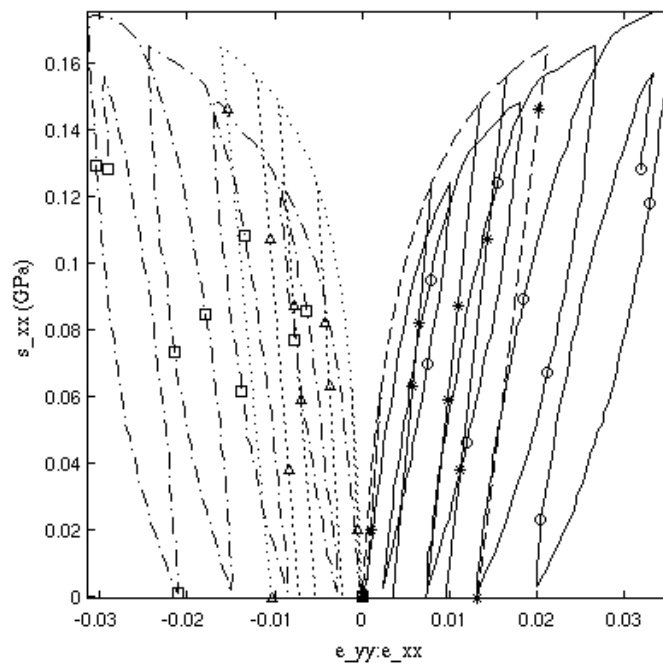
$$\sigma_{11} = 1.7427\bar{\sigma}_x; \quad \sigma_{22} = 0.2943\bar{\sigma}_x; \quad \sigma_{12} = -0.2061\bar{\sigma}_x; \quad (4.2.4)$$

In both the laminae, σ_{22} has a high influence. Thus, due to the difference in the transverse properties (refer table 4.3), the predicted response is stiffer than the experiment. The damage mode in 67.5° lamina is d_3 , whereas, the damage mode in 22.5° lamina is d_2 . This is because, in the 67.5° lamina, σ_{22} is dominant, while in the 22.5° lamina, even though the influence of both σ_{22} and σ_{12} are comparable, the response is due to the fact that the shear damage happens at a lower value of σ_{12} as compared to the transverse damage due to σ_{22} .

The tensile response (figure 4.26) of the modeled transverse matrix crack follows similar trends with that obtained by [4]. The damage mode (d_3) associated with the transverse matrix crack in 67.5° lamina (figure 4.28) has grown five times lesser as compared to [4], this behaviour is as expected because of the nature of damage variable defines in the present case. The 22.5° lamina (figure 4.30) is governed by the damage mode d_2 , which is observed in both the transverse matrix cracks and that of [4].



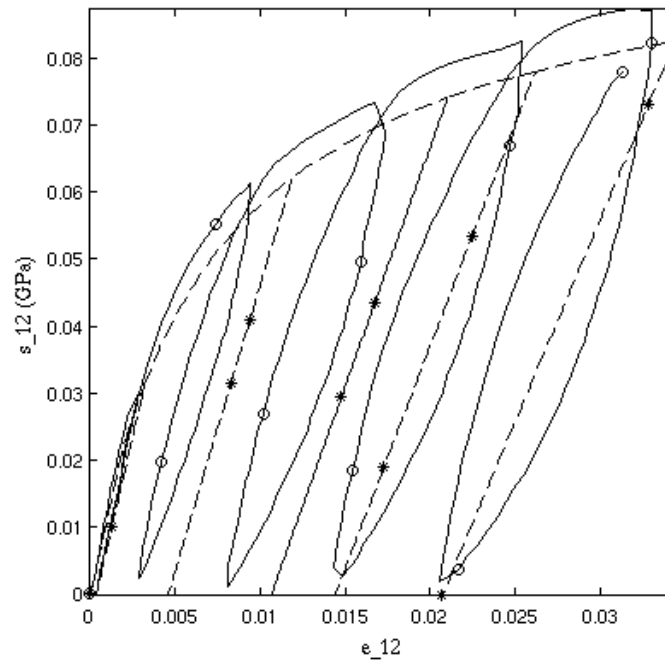
(a) Matrix cracks [4]



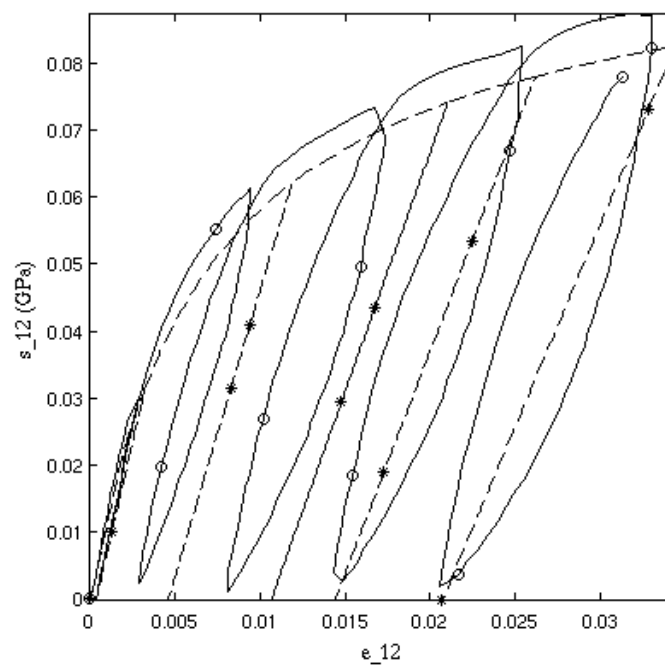
(b) Matrix cracks (present model)

$- \circ -$ experimental (*axial*) $- - * - -$ model (*axial*) $\cdot - \square - \cdot$ experimental (*transverse*)
 $\cdots \Delta \cdots$ model (*transverse*)

Figure 4.2: Prediction of tensile response of $[\pm 45]_s$ T300/914 carbon/epoxy laminates



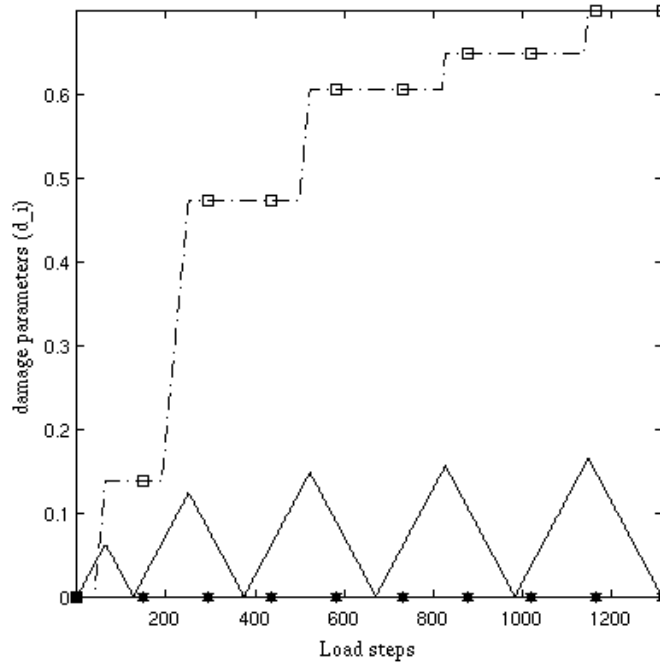
(a) Matrix cracks [4]



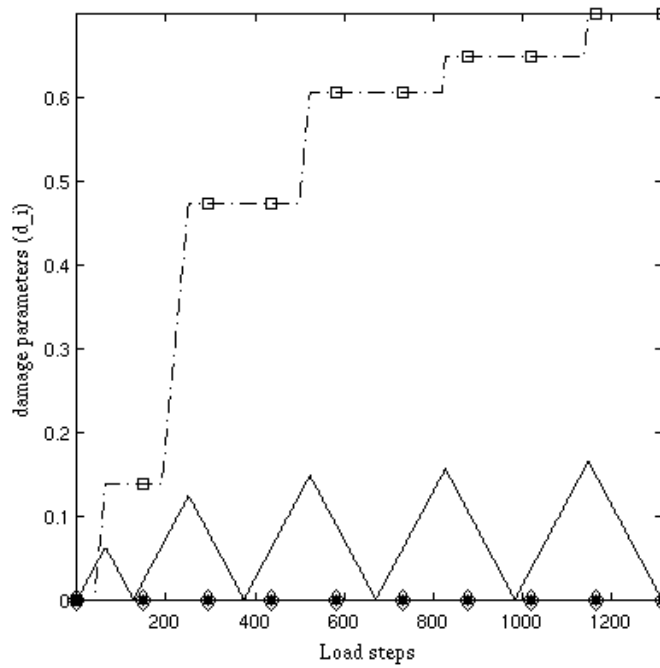
(b) Matrix cracks (present model)

— ○ — experimental — * — — model

Figure 4.4: Prediction of lamina shear response of $[\pm 45]_s$ T300/914 carbon/epoxy laminates



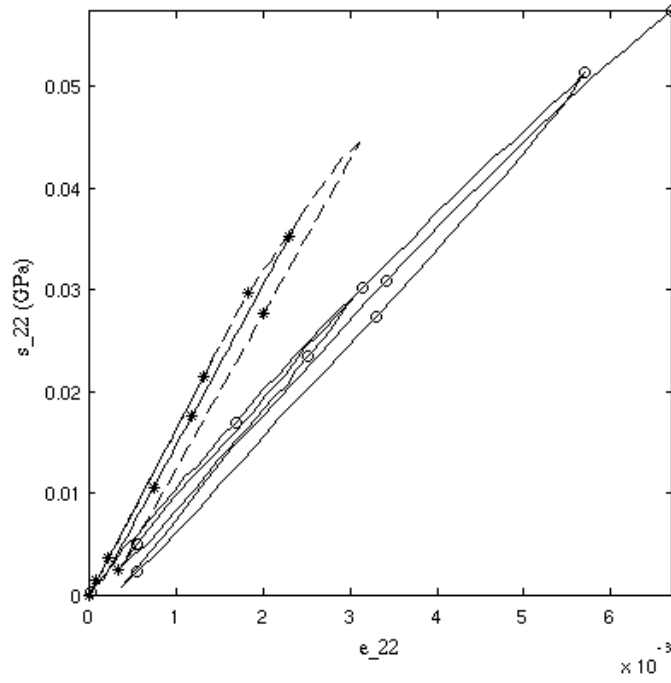
(a) Damage parameters [4]



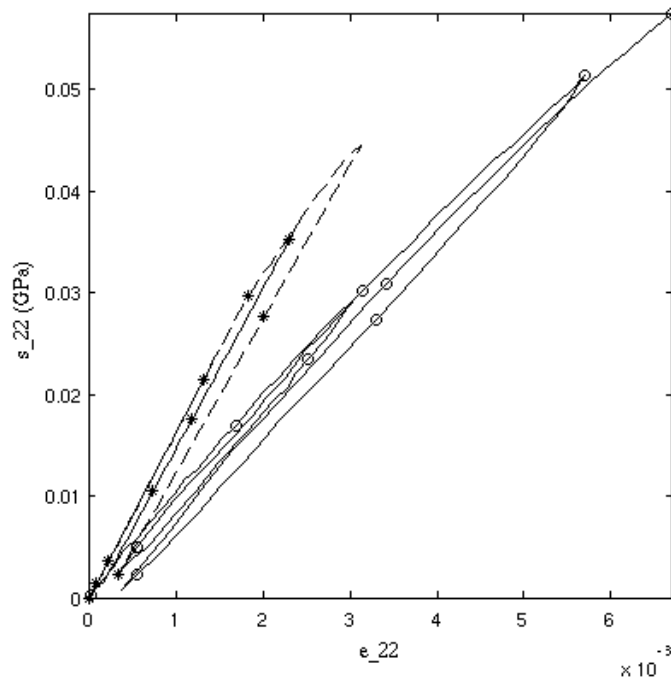
(b) Damage parameters (present model)

— σ_{xx} — * — fiber breakage (d_1) · — □ — fiber/matrix debond (d_2)
 · · · Δ · · · matrix crack (d_3) —◇— matrix crack (d_4)

Figure 4.6: Growth of damage parameters in a lamina of $[\pm 45]_s$ T300/914 carbon/epoxy laminates



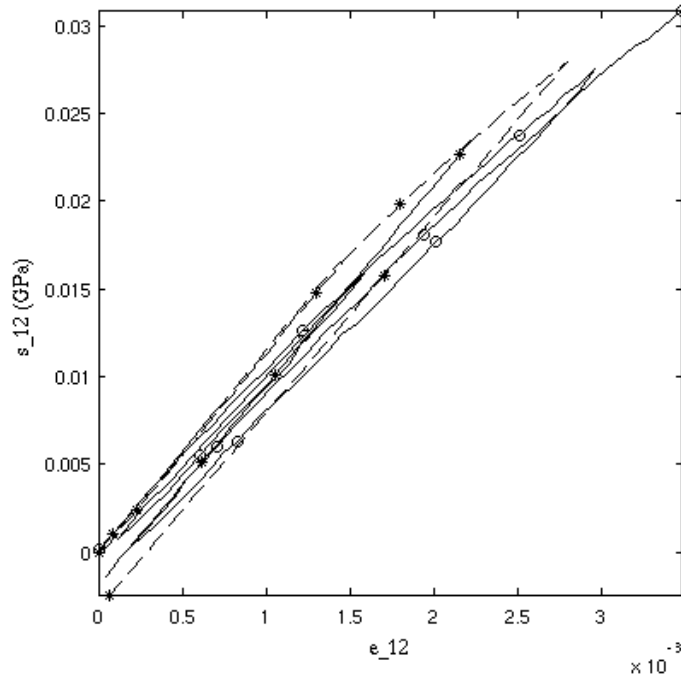
(a) Matrix cracks [4]



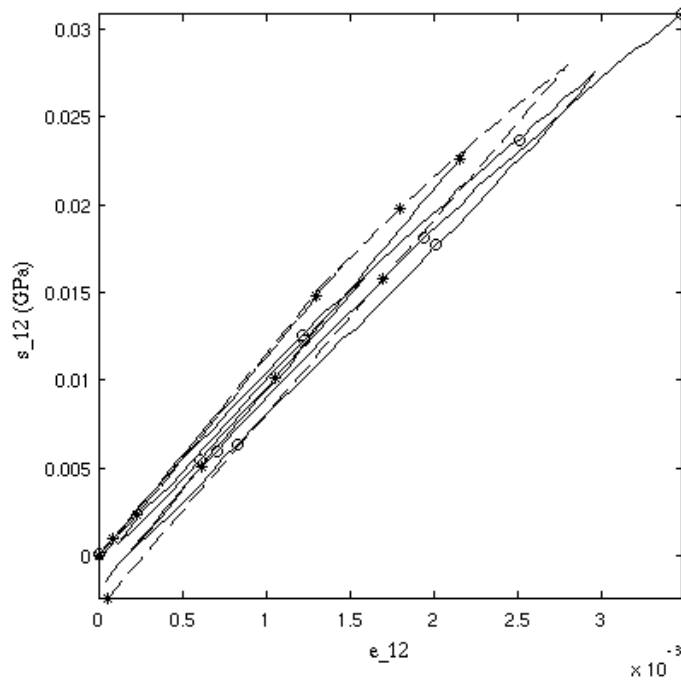
(b) Matrix cracks (present model)

— o — experimental — * — — model

Figure 4.8: Prediction of lamina tensile response of $[\pm 67.5]_s$ T300/914 carbon/epoxy laminates



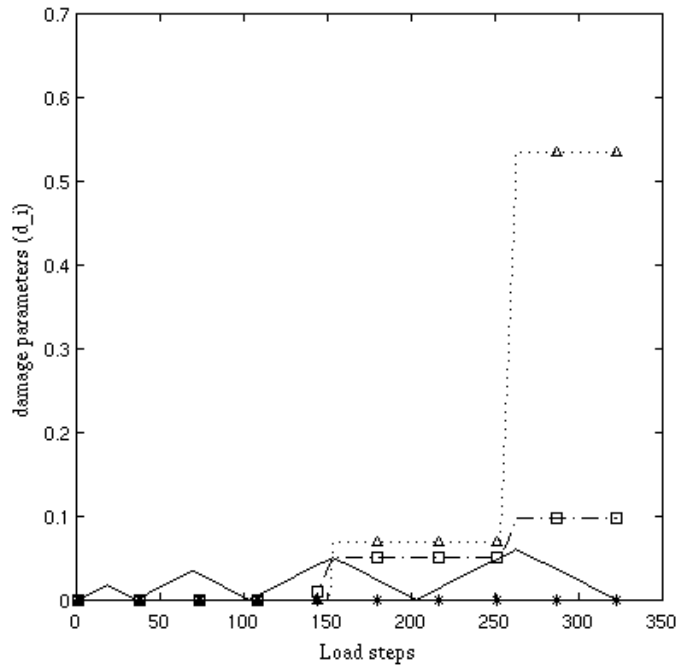
(a) Matrix cracks [4]



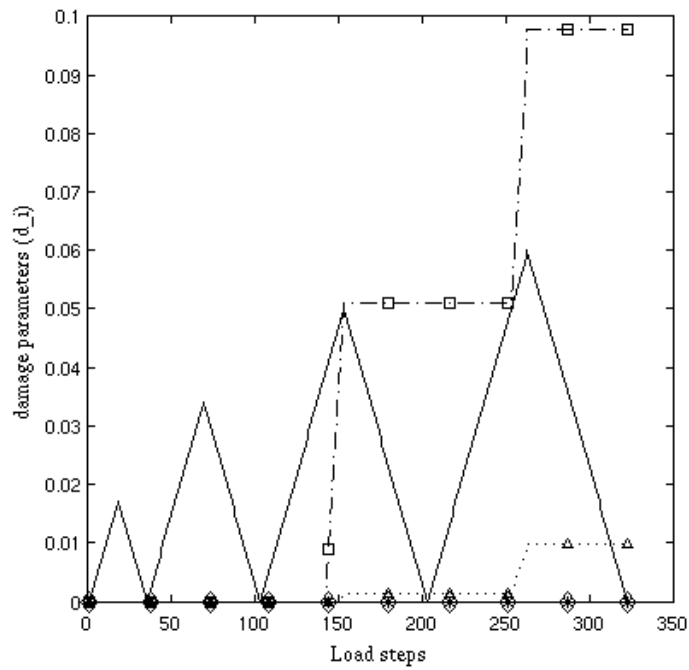
(b) Matrix cracks (present model)

— ○ — experimental — * — — model

Figure 4.10: Prediction of lamina shear response of $[\pm 67.5]_s$ T300/914 carbon/epoxy laminates



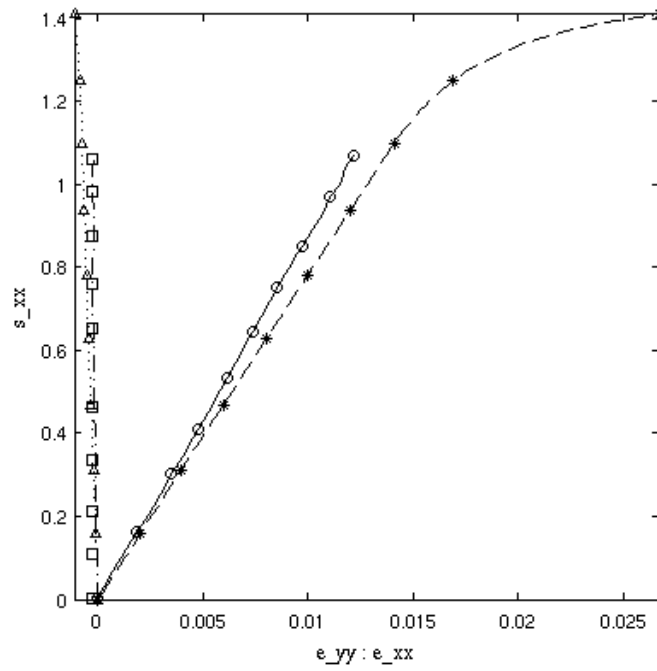
(a) Damage parameters [4]



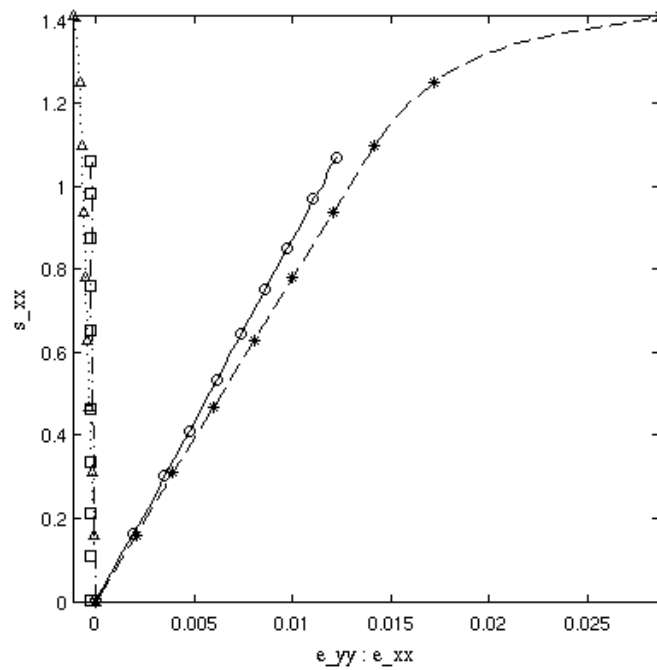
(b) Damage parameters (present model)

— Applied stress (σ_{xx}) — * — fiber breakage (d_1) · - □ - · fiber/matrix debond (d_2)
 · · · Δ · · · matrix crack (d_3) -◇- matrix crack (d_4)

Figure 4.12: Growth of damage parameters in a lamina of $[\pm 67.5]_s$ T300/914 carbon/epoxy laminates



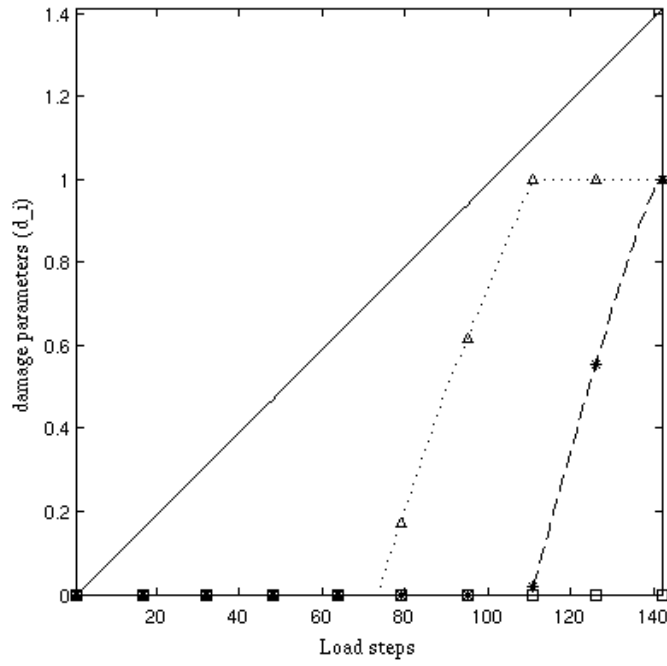
(a) Matrix cracks [4]



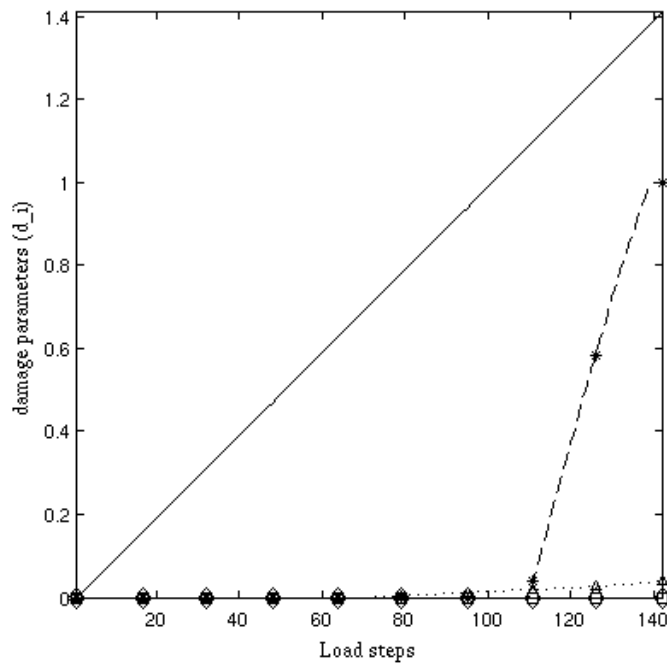
(b) Matrix cracks (present model)

$- \circ -$ experimental (*axial*) $- * -$ model (*axial*) $\cdot - \square - \cdot$ experimental (*transverse*)
 $\cdots \Delta \cdots$ model (*transverse*)

Figure 4.14: Prediction of tensile response of $[0/90]_s$ T300/914 carbon/epoxy laminates



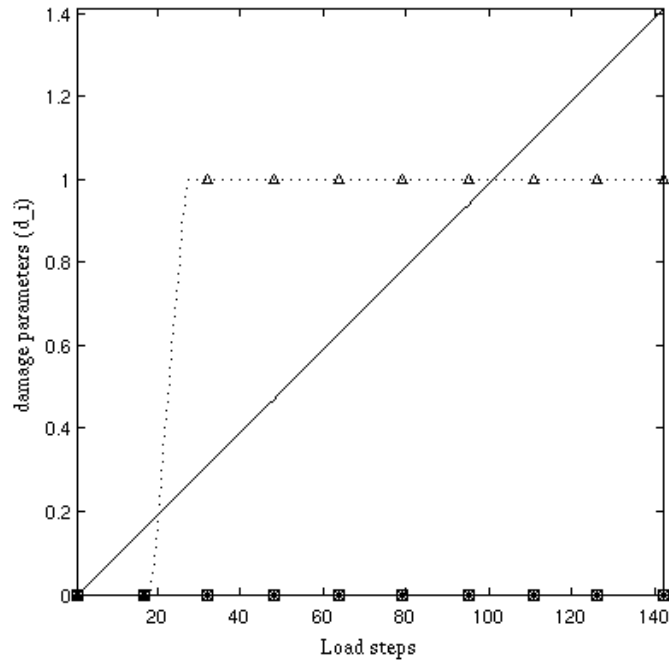
(a) Matrix cracks [4]



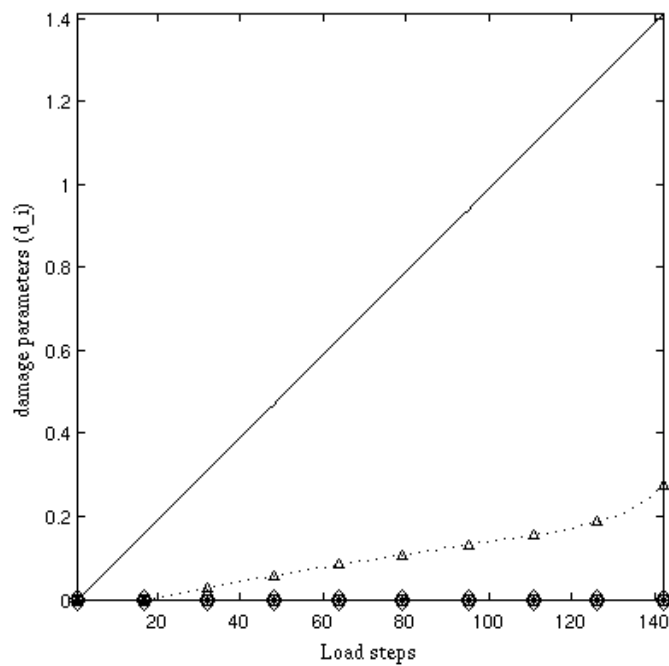
(b) Matrix cracks (present model)

— Applied stress (σ_{xx}) — * — fiber breakage (d_1) · — □ — fiber/matrix debond (d_2)
 ··· Δ ··· matrix crack (d_3) —◇— matrix crack (d_4)

Figure 4.16: Growth of damage parameters in a 0^0 lamina of $[0/90]_s$ T300/914 carbon/epoxy laminates



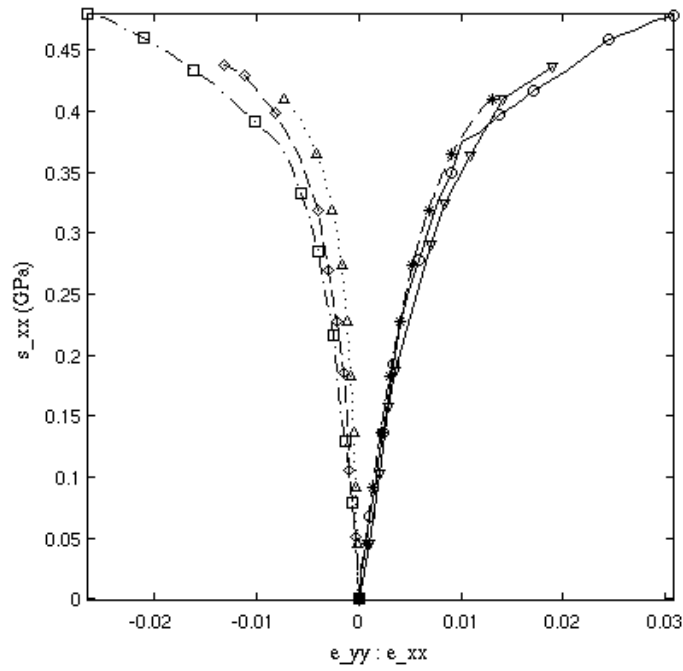
(a) Matrix cracks [4]



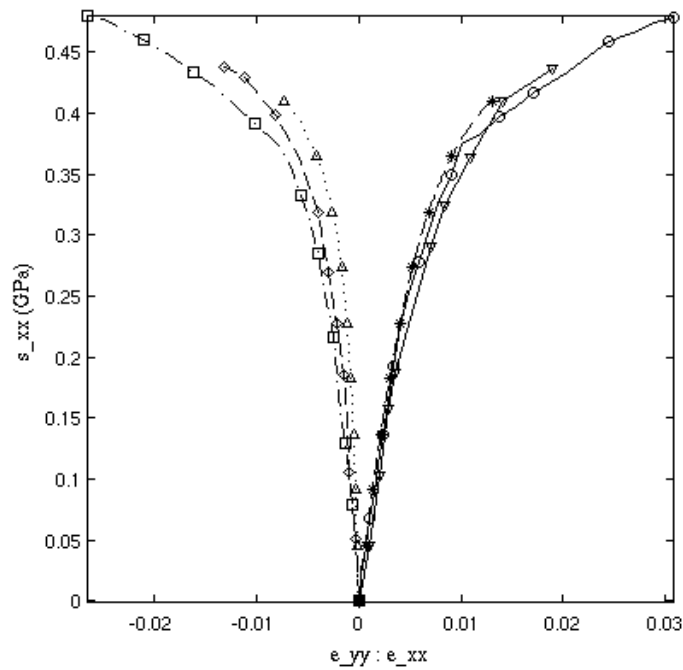
(b) Matrix cracks (present model)

— Applied stress (σ_{xx}) — * — fiber breakage (d_1) · - □ - · fiber/matrix debond (d_2)
 · · · Δ · · · matrix crack (d_3) -◇- matrix crack (d_4)

Figure 4.18: Growth of damage parameters in a 90^0 lamina of $[0/90]_s$ T300/914 carbon/epoxy laminates



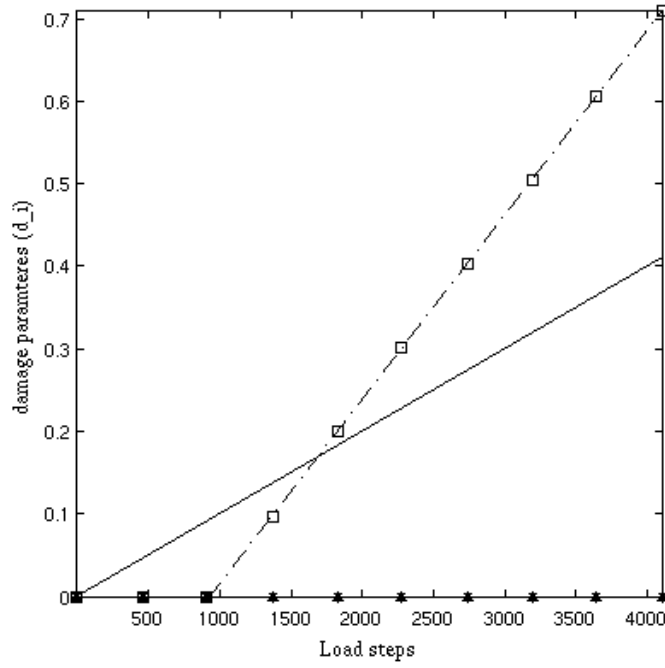
(a) Matrix cracks [4]



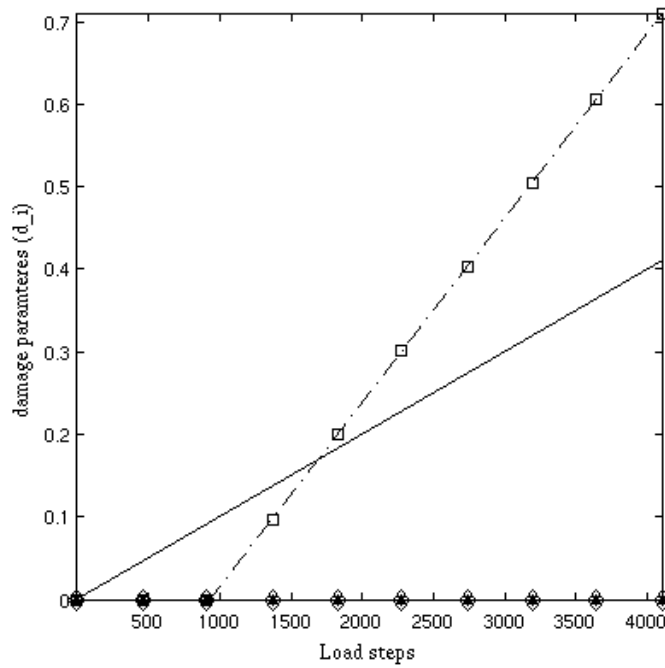
(b) Matrix cracks (present model)

— ○ — experimental (*axial*) — * — model (*axial*) · — □ — experimental (*transverse*)
 · · · Δ · · · model (*transverse*) — ▽ — DML (*axial*) — ○ — DML (*transverse*)

Figure 4.20: Prediction of tensile response of $[-12/78]_{2s}$ T300/914 carbon/epoxy laminates



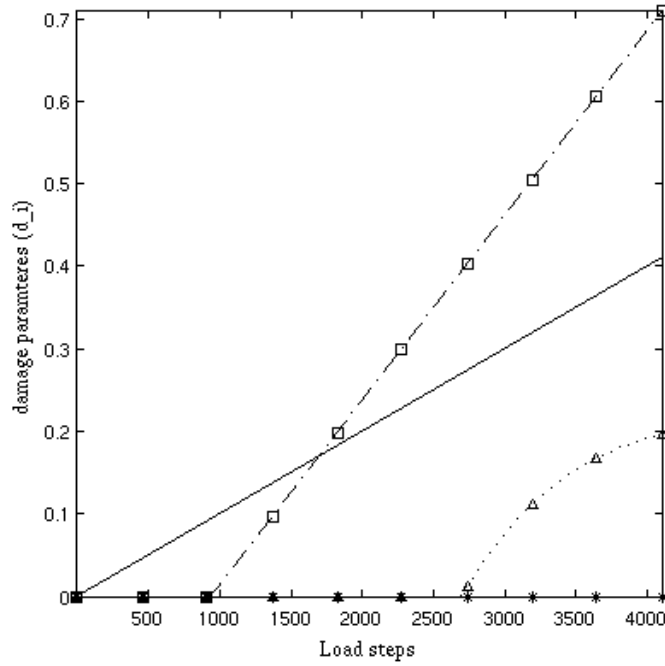
(a) Matrix cracks [4]



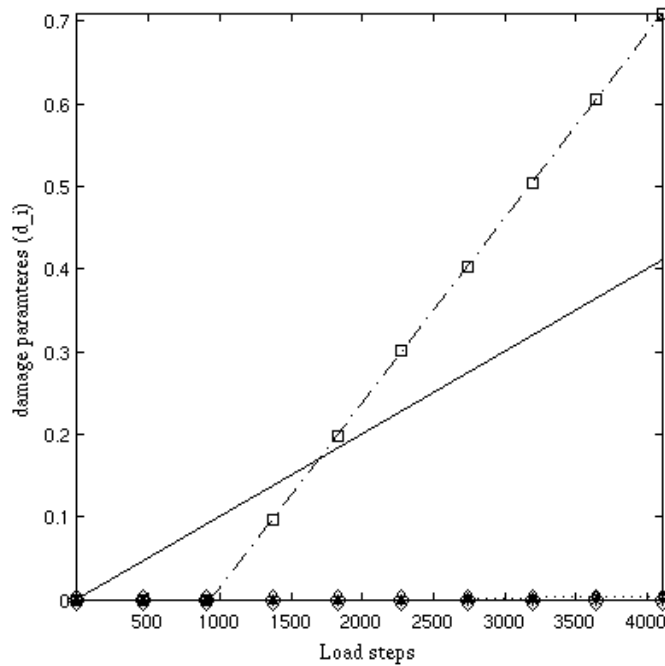
(b) Matrix cracks (present model)

— Applied stress (σ_{xx}) — * — fiber breakage (d_1) · - □ - · fiber/matrix debond (d_2)
 · · · Δ · · · matrix crack (d_3) - \diamond - matrix crack (d_4)

Figure 4.22: Growth of damage parameters in a -12^0 lamina of $[-12/78]_{2s}$ T300/914 carbon/epoxy laminates



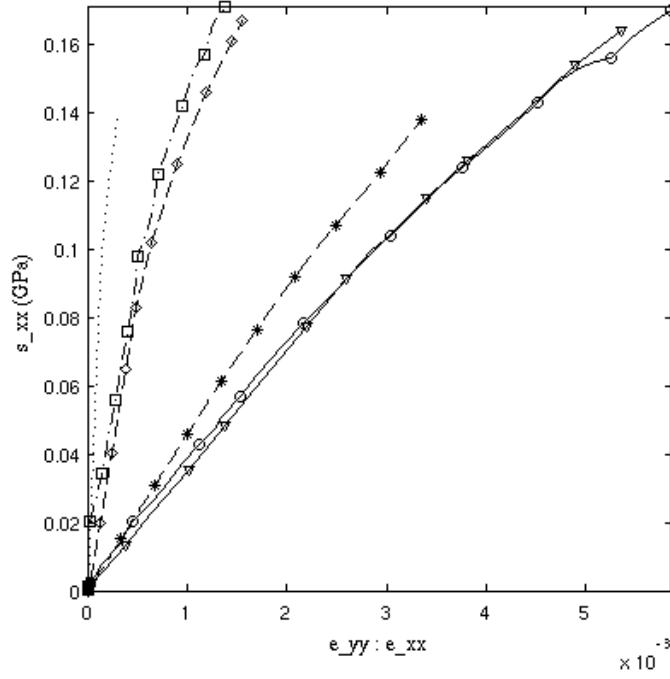
(a) Matrix cracks [4]



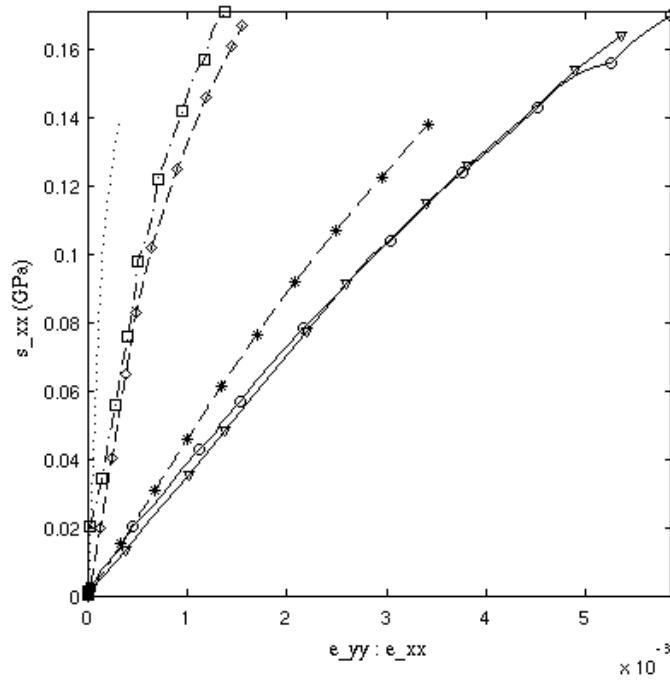
(b) Matrix cracks (present model)

— Applied stress (σ_{xx}) — * — fiber breakage (d_1) · - □ - · fiber/matrix debond (d_2)
 · · · Δ · · · matrix crack (d_3) -◇- matrix crack (d_4)

Figure 4.24: Growth of damage parameters in a 78^0 lamina of $[-12/78]_{2s}$ T300/914 carbon/epoxy laminates



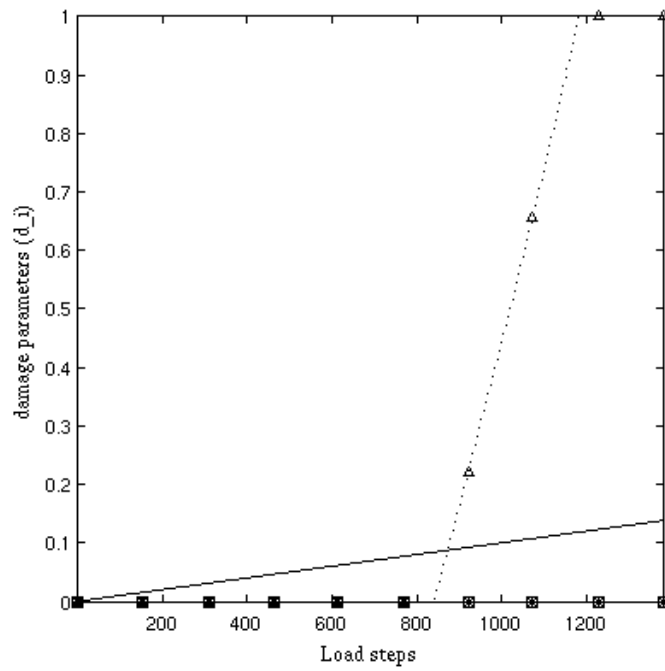
(a) Matrix cracks [4]



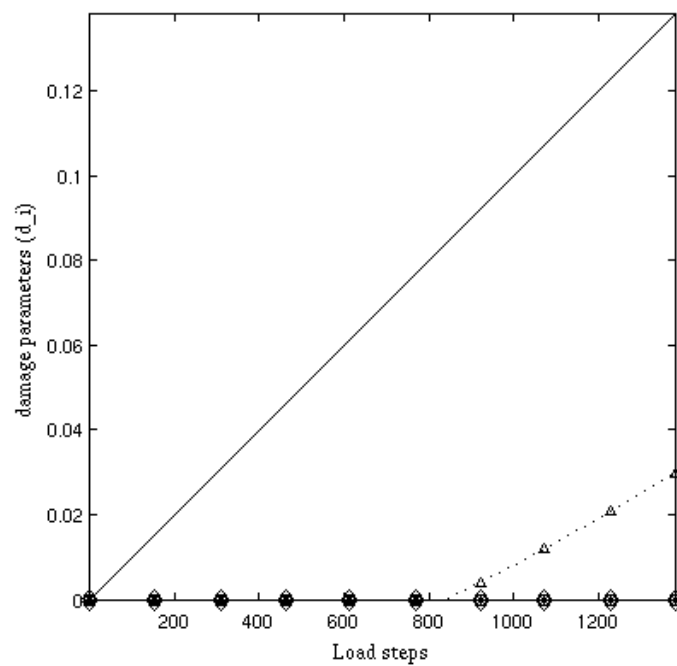
(b) Matrix cracks (present model)

- o - experimental (*axial*) - - * - - model (*axial*) · - □ - · experimental (*transverse*)
 ····· model (*transverse*) - ▽ - DML (*axial*) - - o - - DML (*transverse*)

Figure 4.26: Prediction of tensile response of $[67.5/22.5]_{2s}$ T300/914 ca/ep laminates



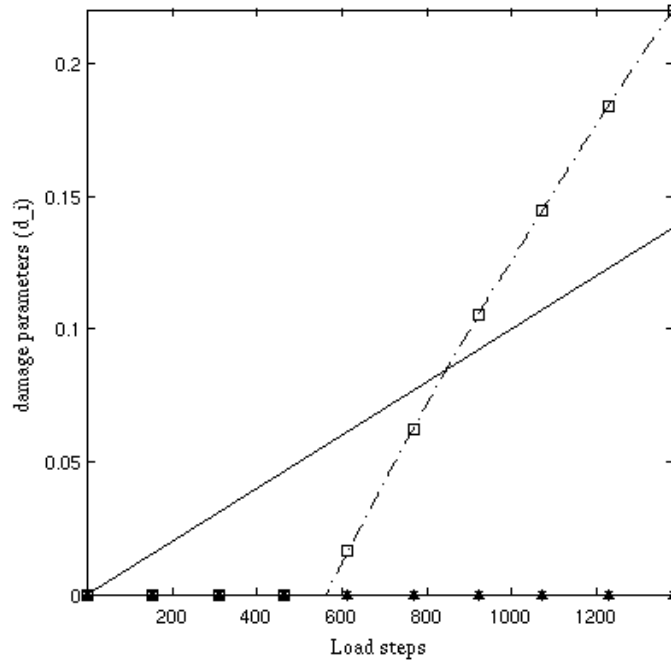
(a) Matrix cracks [4]



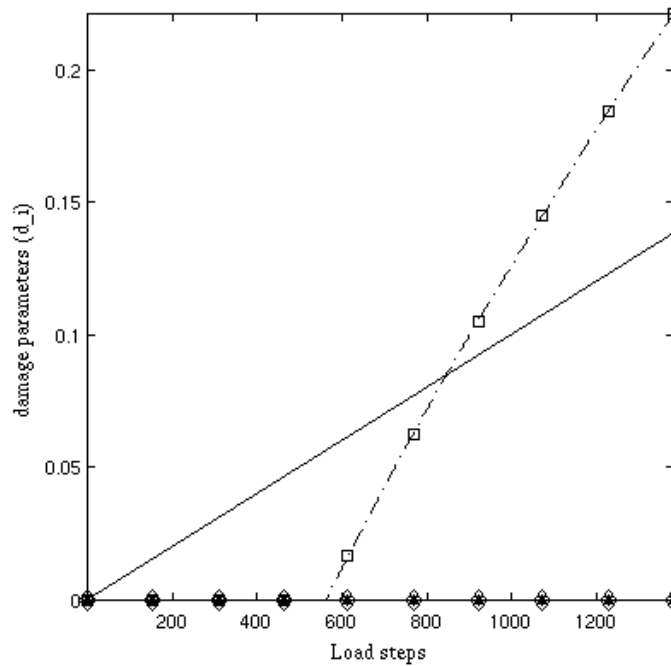
(b) Matrix cracks (present model)

— Applied stress (σ_{xx}) — * — fiber breakage (d_1) · — □ — fiber/matrix debond (d_2)
 ··· Δ ··· matrix crack (d_3) —◇— matrix crack (d_4)

Figure 4.28: Growth of damage parameters in a 67.5° lamina of $[67.5/22.5]_{2s}$ T300/914 ca/ep laminates



(a) Matrix cracks [4]



(b) Matrix cracks (present model)

— Applied stress (σ_{xx}) — * — fiber breakage (d_1) · - □ - · fiber/matrix debond (d_2)
 · · · Δ · · · matrix crack (d_3) -◇- matrix crack (d_4)

Figure 4.30: Growth of damage parameters in a 22.5° lamina of $[67.5/22.5]_{2s}$ T300/914 ca/ep laminates

Chapter 5

Conclusions

5.1 Conclusions

This study is focused on two types of matrix cracks propagating in y and z directions along the length of the RVE with varying damage sizes. Using the mathematical theory of homogenization, a detailed micromechanical analysis at the level of the constituents (fibers and matrix) is conducted for the matrix cracks. Several numerical experiments are performed on unit-cell RVEs to understand the effect of different sizes of assumed matrix cracks on the effective properties of the composites and to study the local state of stresses and strains.

Different kinds of laminates were cyclically and monotonically loaded and studied for the evolution of these matrix cracks in each ply. And there saturation levels were observed. These were further compared with those observed by [4].

The main conclusions of this study are summarized as follows:

1. A better matrix crack model with the actual physics observed based on stress concentration zones was modeled.

2. The damage model [4] under study was effective in capturing the response of wide varieties of composite laminates with the present transverse matrix cracks included.
3. From the micromechanical analysis it is clearly seen that the unit-cell RVE analysis is sufficient to model the normal matrix cracks considered.
4. The dependence of damage behaviour on volume fraction which was previously studied was repeated on transverse matrix cracks, which showed great dependence of damage behaviour on volume fraction.

5.2 Future scope

Some of the possible extensions to this study can be:

1. A complete 3-dimensional analysis including the transverse stress (σ_{33}) can be carried out to get the nature of evolution of the z-direction cracks.
2. A detailed study incorporating the interaction of several damage modes coupled with the transverse matrix cracks can be taken.
3. The present study can be extended to include the evolution of transverse matrix cracks in compression loading.

References

- [1] Carl T. Herakovich. *Mechanics of fibrous composites*. John Wiley and Sons, New York, 1998.
- [2] S.J. Hollister and N. Kikuchi “A comparison of homogenization and standard mechanics analyses for peiodic porous composites.” *Comp. Mechanics*,, 10:73 95, 1992.
- [3] J. Lemaitre and J. L. Chaboche. *Mechanics of solid materials.*, Cambridge university press, Cambridge, 1990.
- [4] V. Murari *Micromechanics Based Continuum Damage Model for Ply Failure in Unidirectional Composites*. PhD Thesis., 2010.
- [5] Pierre Ladeveze. Multiscale computational damage modelling of laminate composites., Course CISM, 2005.
- [6] Jacob Fish and Qing Yu. Multiscale damage modeling for composite materials: theory and computational framework. *International Journal for Numerical Methods in Engineering* ,52:161-191, 2001.
- [7] Somnath Ghosh, Kyunghoon Lee, and Prasanna Raghavan. A multi-level computational model for multi-scale damage analysis in composite and porous materials. *International Journal of Solids and Structures*, 38:2335-2385, 2001.

-
- [8] Flavio V. Souza and David H. Allen. Multi-scale modeling of impact heterogeneous viscoelastic solids containing evolving microcracks. *International Journal for Numerical Methods in Engineering*, 82:464-504, 2010.
- [9] N. Bakvalov and G. Panasenko. *Homogenization: Averaging Processes in Periodic media.*, Springer, 1984.
- [10] Alain Bensoussan, Jacques-Louis Lions, and George Papanicolaou. *Asymptotic Analysis for Periodic Structures.* North Holland Publishing Company, 1978.
- [11] Shaofan Li. *Introduction to micromechanics and nanomechanics - Lecture notes(CE236/C214).* . University of California, Berkeley.
- [12] S. Mall, D.W. Katwyk, R.L. Bolick, A.D. Kelkar, D.C. Davis Tension-compression fatigue behavior of a H-VARTM manufactured unnotched and notched carbon/epoxy composite *Composite Structures* 90 (2009) 201-207.
- [13] B.A. Sjogren, L.A. Berglund The effects of matrix and interface on damage in GRP cross-ply laminates *Composites Science and Technology* 60 (2000) 9-21.
- [14] Peter W.R. Beaumont. Pushing the performance limit of composite structures Part 2: Cracking models *Reinforced Plastics*, Volume 50, Issue 11, December 2006, Pages 30-36.
- [15] Krystyna Imielinska, Laurent Guillaumat. The effect of water immersion ageing on low-velocity impact behaviour of woven aramid-glass fibre/epoxy composites. *Composites Science and Technology* 64 (2004) 2271-2278.
- [16] L. M. Kachanov. *Introduction to continuum damage mechanics.* Martinus Nijhoff publishers, Dordrecht, 1986.
- [17] P. Ladeveze and E. Le Dantec. Damage modelling of the elementary ply for laminated composites. *Composites Science and Technology*, 43:257-267, 1992.

-
- [18] Pierre Ladeveze and Gilles Lubineau. On a damage mesomodel for laminates: micromechanics basis and improvement. *Mechanics of Materials*, 35:763-775, 2003.
- [19] Hinton, M. J., Kaddour, A. S., Soden, P. D. *Failure criteria in fibre reinforced polymer composites: The world-wide failure exercise*, Elsevier Sci Ltd, 2004
- [20] Pierre Ladeveze and Gilles Lubineau. On a damage mesomodel for laminates: micromechanics basis and improvement. *Mechanics of Materials*, 35:763-775, 2003.